CABra: a novel large-sample dataset for Brazilian catchments

André Almagro[1], Paulo Tarso S. Oliveira[1], Antônio Alves Meira Neto[2], Tirthankar Roy[3] & Peter Troch[4]

[1]Faculty of Engineering and Geography, Federal University of Mato Grosso do Sul, Campo Grande, MS, Brazil.
[2]Institute of Climate Studies, Federal University of Espírito Santo, Vitória, ES, Brazil.
5   [3]Civil and Environmental Engineering, University of Nebraska-Lincoln, Omaha, NE, United States.
[4]Department of Hydrology and Atmospheric Sciences, The University of Arizona, Tucson, AZ, United States.

Correspondence to: André Almagro (andre.almagro@gmail.com)

Abstract. In this paper, we present the Catchments Attributes for Brazil (CABra), which is a large-sample dataset for Brazilian catchments that includes long-term data (30 years) for 735 catchments in eight main catchment attribute classes
10   (climate, streamflow, groundwater, geology, soil, topography, land-cover, and hydrologic disturbance). We have collected and synthesized data from multiple sources (ground stations, remote sensing, and gridded datasets). To prepare the dataset, we delineated all the catchments using the Multi-Error-Removed Improved-Terrain Digital Elevation Model and the coordinates of the streamflow stations provided by the Brazilian Water Agency, where only the stations with 30 years (1980-2010) of data and less than 10% of missing records were included. Catchment areas range from 9 to 4,800,000 km² and the
15   mean daily streamflow varies from 0.02 to 9 mm day^{-1}. Several signatures and indices were calculated based on the climate and streamflow data. Additionally, our dataset includes boundary shapefiles, geographic coordinates, and drainage area for each catchment, aside from more than 100 attributes within the attribute classes. The collection and processing methods are discussed along with the limitations for each of our multiple data sources. The CABra intends to improve the hydrology-related data collection in Brazil and pave the way for a better understanding of different hydrologic drivers related to climate,
20   landscape, and hydrology, which is particularly important in Brazil, having continental-scale river basins and widely heterogeneous landscape characteristics. In addition to benefitting catchment hydrology investigations, CABra will expand the exploration of novel hydrologic hypotheses and thereby advance our understanding of Brazilian catchments' behavior. The dataset is freely available at https://doi.org/10.5281/zenodo.4070147.

1 Introduction

25   The integrated assessment of large-sample catchment attributes is fundamental for the description and classification of landscape properties, leading to an improved understanding of similarities (or dissimilarities) between catchments. Large-sample catchment hydrology is essential in terms of hydrological processes understanding (Addor et al., 2020; Beven et al., 2020). It provides an attractive venue for general inferences that would otherwise be impossible to study based on individual or small groups of catchments, aside from allowing the testing of new and existing hypotheses in hydrologic sciences (Addor
30   et al., 2017; Gupta et al., 2014; Lyon and Troch, 2010; Wagener et al., 2007).

A classic example of a large catchment-scale dataset is the Model Parameter Estimation Experiment (MOPEX) (Duan et al., 2006; Schaake et al., 2006), with hydrologic time series from 438 catchments located within the continental US (CONUS). The MOPEX dataset has been used in several studies supporting theoretic and modeling advances in hydrologic sciences (Ao et al., 2006; Ren et al., 2016; Sawicz et al., 2011). A more recent example is the Catchment Attributes and

35 MEteorological for Large-sample Studies (CAMELS, Addor et al. (2017)) consisting of a set of daily hydrometeorological time series data for 671 small- to medium-sized catchments for the CONUS, aside from several landscape and climate related attributes. The CAMELS initiative has been widely used and other large-sample datasets have been recently developed following the CAMELS format, such as CAMELS-GB for Great Britain, covering 671 catchments and CAMELS-CL for Chile, covering 516 catchments. A list of available large-sample datasets can be found in Addor et al. (2020).

40 Brazil is a country with continental dimensions, hosting a wide range of climates, soils, geology, and land-cover types. Despite covering almost 50% of South America and hosting between 12% and 18% of the world's renewable freshwater (Rodrigues et al., 2015; UNEP and ANA, 2007), Brazil suffers from scarce allocation of funds for hydrological monitoring services, which creates great challenges for the proper monitoring of the quality and quantity of its water resources. While the density of streamflow gauges falls below the standards than recommended by the World Meteorological Organization

45 (WMO) of 1 station for each 1,000 km², hydrologic observations are often discontinued and lack proper length (ANA, 2019; WMO, 2010). Additionally, there is no repository for other relevant landscape-related variables (e.g., land-cover, groundwater, geology, or soil type). An integrated dataset containing multiple levels of environmental information can be of extreme importance to leverage investigations in hydrology and related disciplines within the Brazilian territory.

Recently, two large-sample datasets for catchment attributes have been simultaneously developed for Brazil: the Catchment

50 Attributes for Brazil (CABra) (introduced in Oliveira et al., 2020) and the Catchment Attributes and MEteorology for Large-sample Studies (CAMELS-BR) (Chagas et al., 2020). Even though both datasets aim to fill the lack of hydrological data access in Brazil, the data sources, quality control, number, and types of attributes differ significantly. To address the similarities and differences between both datasets, an extensive discussion comparing CAMELS-BR and CABra is also presented in our study.

55 In this paper, we present the CABra dataset, which is a comprehensive, large-sample dataset for catchment attributes in Brazil. We have synthesized several multi-source data from eight main attribute classes (topography, climate, streamflow, groundwater, soil, geology, land-use and land-cover, and hydrologic disturbance) for 735 catchments in Brazil. Our dataset covers all Brazilian administrative and hydrographic regions as well as its biomes. We have delimited all the catchments using an error-corrected digital elevation model employing automatic drainage area delineation methods. For the area-

60 averaged attributes, we have used national datasets from the Brazilian Water Agency (ANA), Brazilian Agricultural Research Corporation (EMBRAPA), and Xavier et al. (2016), and widely used global datasets, such as ERA5, SoilGrids250, Global Land Evaporation Amsterdam Model (GLEAM), Global Lithologic Map (GLiM), and GLobal HYdrogeology MaPS (GLHYMPS). Additionally, a hydrologic disturbance index was created to indicate the most human-impacted catchments. Finally, we discuss the spatial variabilities of the attributes and their limitations of application.

2 The CABra dataset

2.1 Overview

The CABra dataset is a multi-source, multi-temporal, and multi-spatial resolution large-sample dataset for catchment attributes for Brazilian catchments. Using an extensive local/global high-quality data collection, we developed CABra considering eight main classes of attributes: topography, climate, streamflow, groundwater, soil, geology, land-cover, and hydrological disturbance. Gridded datasets of various kinds were averaged onto the selected catchments located over Brazil and neighboring countries, in the case of transboundary catchments. Moreover, we provide daily time series from climate and streamflow variables for a 30-year period, covering the hydrological years from 1980 to 2010, as described in Fig. 1.
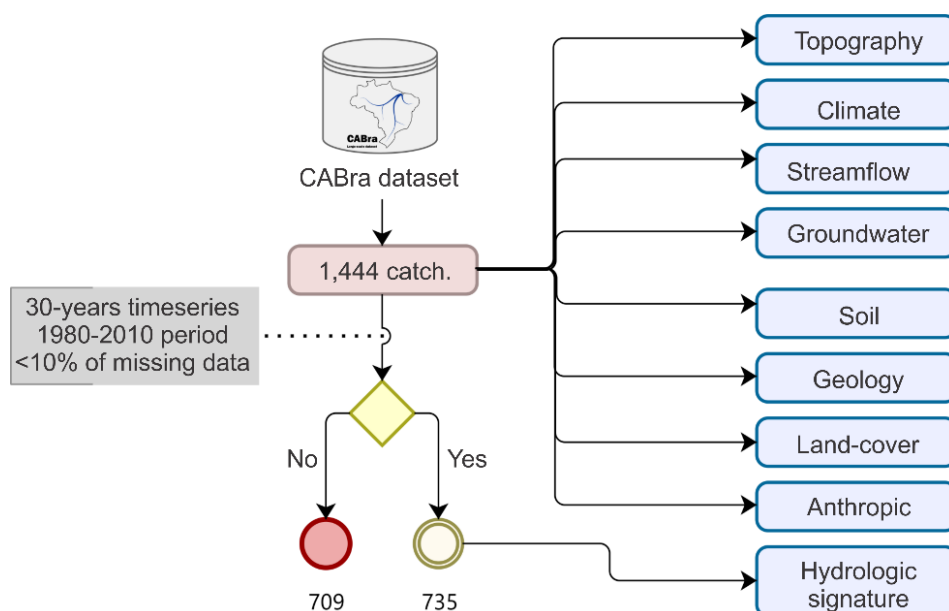
Figure 1: Study delineation for the CABra dataset organization. From 1,444 catchments from ANA's database, 735 were selected to integrate our dataset due to its high consistency and long time series of streamflow.

The CABra dataset is recommended for a wide range of users for decision-making at multiple scales – local, national, or regional – covering all Brazilian biomes (Amazon, Cerrado, Atlantic Forest, Pantanal, Caatinga, and Pampa). CABra was created to ensure easy access to its information and provide high-quality data, with attributes useful for a variety of hydrometeorological modeling and assessments. Each catchment presents several attributes, ranging from the file information described in Table 1 to the attributes described throughout this article. Moreover, we made available all the geospatial data (shapefile of the boundaries) for the users.

Table 1: General attributes of the CABra catchments.

Type	Attribute	Long name	Unit
Identification	cabra_id	CABra's identification code of the streamflow gauge	-
	ana_id	ANA's identification code of the streamflow gauge	-
Location	longitude	Longitude coordinate of the streamflow gauge	dd
	latitude	Latitude coordinate of the streamflow gauge	dd
	gauge_hreg	The Brazilian hydrographic region of the streamflow gauge location	-
	gauge_biome	The Brazilian biome of the streamflow gauge location	-
	gauge_state	The Brazilian state of the streamflow gauge location	-
Quality	missing_data	Percentage of missing data	%
	series_length	Timeseries length of the streamflow gauge	years
	quality_index	Quality index of the CABra catchment	-

- Means dimensionless

2.2 Catchment delineation and topography

90 Brazil does not have an official database for the national catchments boundaries, and the Brazilian Water Agency (ANA) does not make available its geospatial database. Because of this and to avoid uncertainties in the existing datasets for South America, we freshly generated all the CABra catchments boundaries used in this study. Digital Elevation Model (DEM) quality and resolution are crucial at this stage since all the post-analysis with the multi-source information utilized in the CABra dataset are area-averaged. For example, is well-known that errors in topographic indices, e.g., slope and catchment

95 area and boundary, are dependent on and highly sensitive to DEM resolution and accuracy, and it is suggested that, if available, a high-resolution DEM should be used instead of a low-resolution DEM due the negative effects of terrain generalization caused by them (Mukherjee et al., 2012; Vaze et al., 2010; Wechsler, 2007; Zhou and Liu, 2004). We delineated the CABra catchments following the procedure described in Maidment (2002), using streamflow gauges location information from the ANA's database and a high-resolution elevation product, i.e., the Multi-Error-Removed Improved-

100 Terrain Digital Elevation Model with a 90-m spatial resolution at Equator (Yamazaki et al., 2017) (Fig. 2).
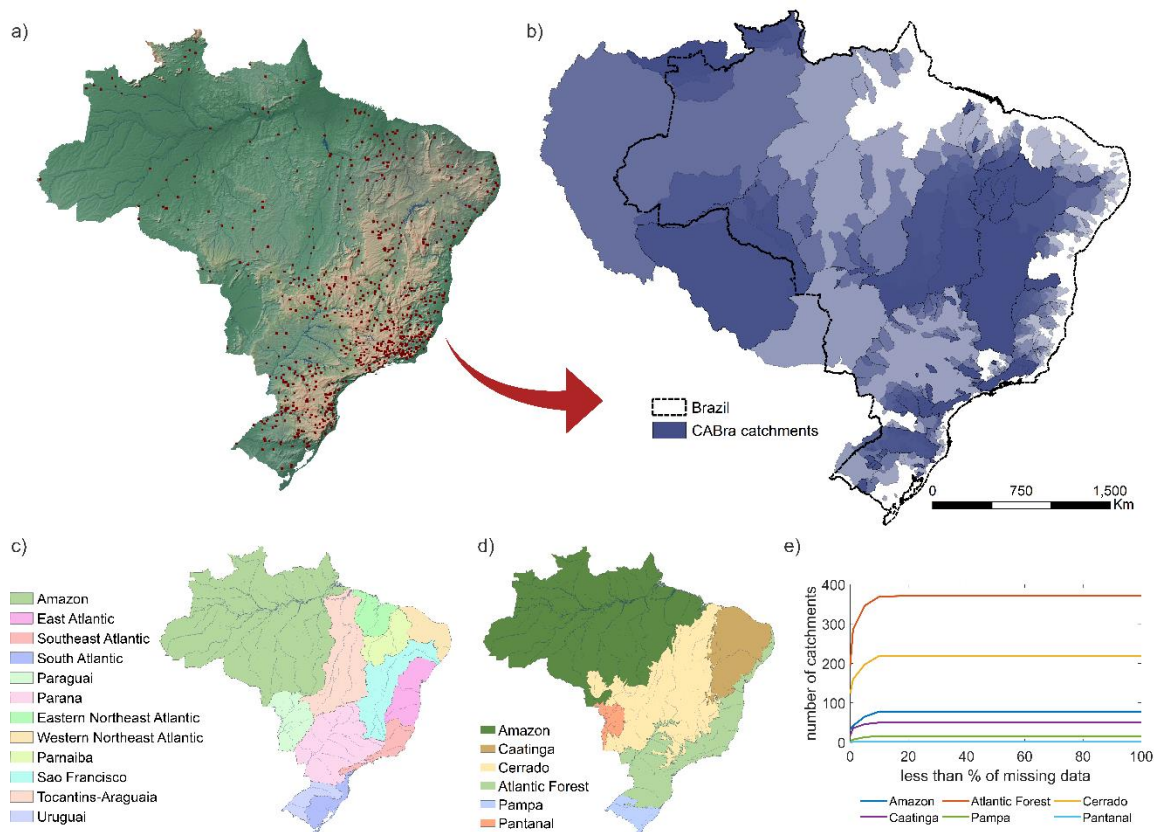
Figure 2: Location map of the streamflow gauges and CABra catchments. a. Streamflow gauges coordinates of CABra catchments; b. The 735 CABra catchments boundaries; c. The 12 hydrographic regions of Brazil; d. The six main biomes of Brazil; e. Level of consistency of the streamflow gauges records for each biome.

105

In the first stage, which we call "terrain processing", the DEM was sink-filled to avoid possible errors due to peaks or depressions. Then, the flow direction and flow accumulation were calculated, which indicates the direction and accumulation of flow, respectively, in each grid cell within the catchment. The next step was to define the stream network in the catchment. For the definition of a river stream, we considered a threshold of 100 cells accumulating water, and this value

110   was chosen considering the DEM spatial resolution and the range of the size of the catchments. All the previous steps were run for the South America extension. Even though all outlets are located in the Brazilian territory, some of the drainage areas embrace larger areas outside of it.

The second step was catchment delineation, where the products generated in the previous step and the coordinates of the streamflow gauges were used. Each streamflow gauge coordinate was first plotted as a point and the position of it to the

115   stream network was checked and corrected, if necessary. The correction procedure was performed for 132 out of CABra catchments. Then, each corrected point was used as an outlet of the catchment and the delineation of the drainage area was

performed using the ArcHydro tool. Aside from the catchments limits, perimeters, and areas, we also extracted the stream information, such as the stream network and hierarchy (Strahler, 1952, 1957). It is important to highlight that we manually inspected each catchment outlet and area to overcome the limitation of unchecked boundaries of another existing catchment

120 dataset in Brazil (CAMELS-BR, by Chagas et al., 2020) and South America (Do et al., 2018), which were based on a DEM with a spatial resolution of 500-m. Moreover, this presented itself as a crucial procedure for an accurate delineation since several outlets' positions needed to be corrected to represent the real expected catchment boundary.

Once the catchment boundaries were delimited, we calculated six attributes related to the topography of each catchment: area, slope, maximum, minimum, and mean elevation, and streamflow gauge elevation.

125

Table 2: Topography attributes of the CABra catchments.

Type	Attribute	Long name	Unit
Elevation	elev_mean	Mean elevation of the catchment	m
	elev_max	Maximum elevation of the catchment	m
	elev_min	Minimum elevation of the catchment	m
	elev_gauge	Elevation of the streamflow gauge	m
Area	catch_area	Area of the catchment	km²
Slope	catch_slope	Mean slope of the catchment	%
Drainage	catch_order	Order of the catchment based on the Strahler method	

Figure 3 summarizes the topographic attributes for the CABra catchments. Catchment areas ranged from 9 to 4.8×10^6 km² (Fig. 3a). This large range of areas shows how Brazilian hydrology can be, at the same time, local and continental,

130 necessitating a better understanding of hydrologic processes. Many of the largest catchments are in the mainstream of one of the 12 hydrologic regions of Brazil, especially in the Amazon, Tocantins/Araguaia, São Francisco, Paraguay, and Paraná. The mean elevation of CABra catchments ranges from close to zero to up to 2000 m, with the highest values found in the southern and south-eastern portions.

In turn, steepen areas can be found in the coastal and mountainous areas of the southeast and south (Fig. 3b and Fig. 3c).

135 Most of the Brazilian catchments have a flat topography though, with a mean slope up to 10%. Figure 3d shows the gauge elevation. Note the difference between the gauge elevation and the mean catchment elevation in Fig. 3b. The gauge elevation considers only the elevation at the gauge position in the landscape, thereby proving only the local information, while the mean catchment elevation considers the average elevation for the entire catchment. An example of this difference is the largest CABra catchment, i.e., the Amazon. The mean elevation in the Amazon basin would be low, however, the western

140 part of the basin has some of the highest peaks of the Andes, where the gauge elevation would be much higher.
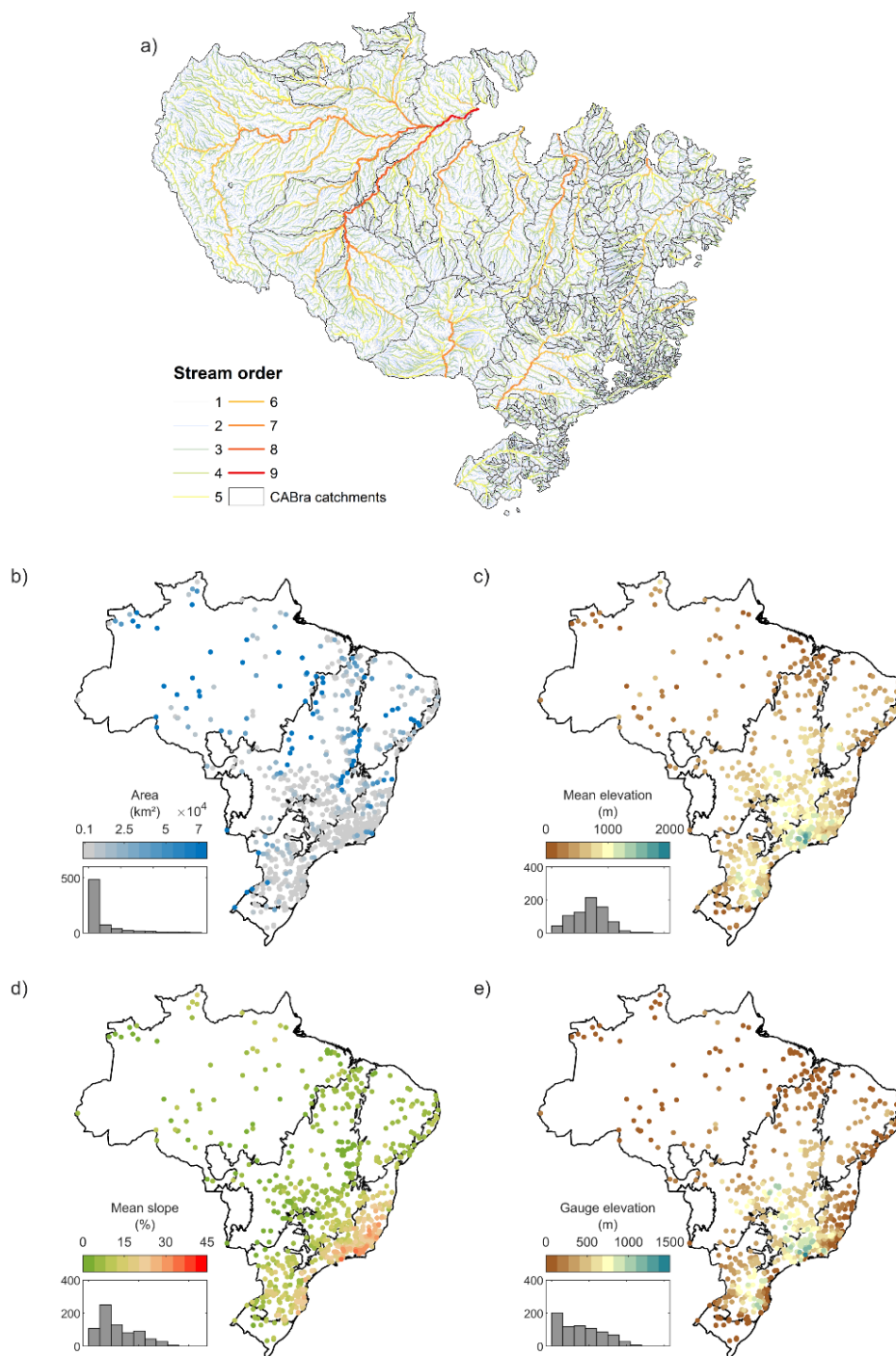
Figure 3: Spatial distribution of the topography attributes of the CABra catchments. a. Stream order of Brazilian rivers; b. Area of the catchments, in km²; c. Mean elevation of the catchments, in m; d. Mean slope of the catchments, in percentage; e. Elevation of the streamflow gauge, in m.

2.3 Climate

2.3.1 Methodology

145

We present daily time series of area-averaged precipitation, minimum, maximum, and mean temperatures, solar radiation, relative humidity, wind speed, evapotranspiration, and potential evapotranspiration (calculated by Penman-Monteith, Priestley-Taylor, and Hargreaves methods). Moreover, we calculated several core climate indices, defined by the Climate

150 and Ocean: Variability, Predictability, and Change project from the World Climate Research Programme (WCRP). Two main climate datasets were used in CABra. The first one, a high-resolution meteorological gridded dataset (0.25ºx0.25º), developed by Xavier et al. (2016) (here referred to as "REF") is based on the spatial interpolation of meteorological data from ~4,000 rain gauges and wheatear stations in Brazil, from the ANA, Brazilian Institute for Meteorology (INMET, in Portuguese), and Water and Power Department of São Paulo (DAEE/SP, in Portuguese), covering the period from 1980 to

155 2015. From these sets of meteorological gauges, 2890 are limited to precipitation data. This dataset is available at http://careyking.com/data-downloads/. This product has a much finer spatial resolution and is based on a higher number of rain gauge stations than other widely used products (~4,000 stations for Brazil, in comparison to ~600 stations for South America in CRU TS3.1 product). However, the REF dataset covers only the Brazilian territory, while the CABra dataset has 20 catchments with upstream areas outside Brazil. To overcome this, we incorporated the ERA5 (Hersbach et al., 2020)

160 climate data into the CABra dataset (here referred to as "ERA5").

ERA5 is the most recent version of climate reanalysis from the European Centre for Medium-Range Weather Forecasts (ECMWF) and provides hourly, daily, and monthly data on several atmospheric, sea, and land variables in a 0.25ºx0.25º spatial resolution grid, from 1950 to the present. As a reanalysis dataset, the ERA5 uses past observations and models to generate accurate and consistent time series of climate variables and parameters, being one of the widely used datasets in

165 geosciences (Hersbach et al., 2020). To incorporate and produce a more reliable product for all the CABra catchments, we have generated an ensemble mean product (here referred to as "ENS") using both datasets beforementioned, i.e., REF and ERA5 climate products. The procedure was conducted in the Climate Data Operators (CDO, Schulzweida, 2019) and aimed to a better characterization and representation of the climate based on the two independent estimations, which imply in a more robust reproducibility of the phenomenon than in a single-member analysis (Abramowitz et al., 2018). The

170 precipitation seasonality (Woods, 2009), which indicates the timing of the precipitation seasonal cycle and the temperature seasonal cycle – values close to +1 indicates summer precipitation and values close to -1 indicates winter precipitation – was calculated for the ensemble product.

The actual evapotranspiration adopted in CABra is derived from the Global Land Evaporation Amsterdam Model version 3 (GLEAM v3, Martens et al., 2017), which is a set of algorithms that estimates the many components of land evaporation

175 based on satellite observations of climatic and environmental variables. The calculations of the actual evapotranspiration by GLEAM v3 take into account a potential evapotranspiration module (by Priestley and Taylor method), an interception loss module (by a Gash analytical model), and a stress module (by a semi-empirical relationship to root-zone moisture and

vegetation optical depth). The GLEAM dataset is one of the most commonly used datasets on evapotranspiration applications (Forzieri et al., 2018; Schumacher et al., 2019; Zhang et al., 2016).

180 Even though the REF dataset presents a reference evapotranspiration product (calculated by Penman-Monteith method following the FAO-56 guidelines), it embraces only the Brazilian territory and did not comprise all the areas of the catchments included in the CABra dataset. To overcome this limitation, we calculated the daily potential evapotranspiration (PET) by three different widely used methods based on energy balance and transfer mass, radiation, and temperature, using meteorological variables from the ERA5 and the ensemble products as inputs. The first method was the FAO-56 Penman-

185 Monteith equation (Allen et al., 1998), which is the standard for reference evapotranspiration, and assumes a hypothetical crop similar to a surface of small grass of uniform grass, actively growing and sufficiently watered. The FAO Penman-Monteith (PM) equation considers the energy budget and the aerodynamic and surface resistances of the crop and uses as inputs the solar radiation, air temperature, humidity, and 2m wind speed data (Equation 1).

$$PET_{PM} = \frac{0.408\Delta(R_n-G)+\gamma\frac{900}{T+273}u_2(e_s-e_a)}{\Delta+\gamma(1+0.34u_2)} \, , \tag{1}$$

190 where PET_{PM} is the reference evapotranspiration, in mm day^{-1}, R_n is the net radiation, in MJ m^{-2} day^{-1}, G is the soil heat flux, in MJ m^{-2} day^{-1}, T is the mean daily temperature at 2m height, in ºC, u_2 is the wind speed at 2m height, in m s^{-1}, e_s is saturation vapor pressure, in kPa, e_a is the actual vapor pressure, in kPa, Δ is the slope vapor pressure curve, in kPa ºC^{-1}, and γ is the psychrometric constant, in kPa ºC^{-1}.

The radiation-based method chosen for the CABra dataset is the Priestley-Taylor equation (PT) (Priestley and Taylor, 1972).

195 The PT considers that when large areas, such as catchments, are saturated, the main force that governates the evaporation is the net radiation, and under certain conditions, the knowledge of net radiation and the ground dryness is enough to determine the vapor and sensible heat fluxes at the surface. Moreover, is one of the most commonly used models to estimate evapotranspiration due to its low number of inputs requirement (Maes et al., 2018; McMahon et al., 2013; Shuttleworth, 1996). The PT equation takes the following form:

200 $$PET_{PT} = \alpha\frac{\Delta}{\Delta+\gamma}(R_n - G) \, , \tag{2}$$

where PET_{PT} is the potential evapotranspiration, in mm day^{-1}, α is the Priestley-Taylor constant, dimensionless, R_n is the net radiation, in MJ m^{-2} day^{-1}, G is the soil heat flux, in MJ m^{-2} day^{-1}, Δ is the slope vapor pressure curve, in kPa ºC^{-1}, and γ is the psychrometric constant, in kPa ºC^{-1}. Considering that PT only considers daytime evapotranspiration and G is negligible during the daytime, we used $G = 0$ in our calculations.

205 The main limitation on the application of the PT method is the requirement of the Priestley-Taylor constant α, which is related to the ratio between the actual evapotranspiration and the equilibrium evaporation rate (Eichinger et al., 1996). Priestley & Taylor (1972) empirically determined α for many locations and conditions in the world, ranging between 1.08

and 1.34. The authors concluded the best estimation for α should be an overall mean of 1.26. However, it is known that the α value is scenario-dependent and its variability is not taken into account when using the mean value proposed in its
210 development (Guo et al., 2007).

The third method adopted here is the Hargreaves equation. The method was developed by Hargreaves (1975) for irrigation planning and design and it is a temperature-based equation widely used to calculate the potential evapotranspiration due to its easy application and low inputs requirement (Equation 3).

$$PET_{HG} = 0.0135 \, R_s (T_a + 17.8),\tag{3}$$

215 where PET_{HG} is the potential evapotranspiration, in mm day^{-1}, R_s is the solar radiation, in MJ m^{-2} day^{-1}, and T_a is the daily mean temperature, in °C.

The main limitation of this equation is the estimative are subject to error due to a large range of temperatures caused by weather fronts on a daily scale. On the other hand, it is a less biased model, when compared to other methods, when applied to small and not well-watered catchments (Hargreaves and Allen, 2003).

220 From the climatic variables and attributes, we carried out an analysis of the annual water balance in the Budyko space, an empirical approach applied to the study of the hydrological behavior of catchments. The Budyko hypothesis (Budyko, 1948, 1974) considers that the ratio between the long-term annual actual evapotranspiration (ET) and precipitation (P) is a function of the ratio between the long-term potential evapotranspiration (PET) and precipitation (P). The Budyko framework has been used to assess global impacts of climate change on water resources (Berghuijs et al., 2017; Roderick et al., 2014), and to gain
225 further insight on water balance controls at mean annual timescales (Donohue et al., 2007; Berghuijs et al., 2017; Meira Neto et al., 2020).

Table 3: Daily series of meteorological variables and climate indices for the CABra catchments.

Type	Attribute	Long name	Unit
Precipitation	p_ref	Mean daily precipitation from the REF	mm day^{-1}
	p_era5	Mean daily precipitation from the ERA5	mm day^{-1}
	p_ens	Mean daily precipitation from the ENS	mm day^{-1}
Temperature	tmax_ref	Max daily temperature from the REF	ºC
	tmin_ref	Min daily temperature from the REF	ºC
	tmax_era5	Max daily temperature from the ERA5	ºC
	tmin_era5	Min daily temperature from ERA5	ºC
	tmax_ens	Max daily temperature from the ENS	ºC
	tmin_ens	Min daily temperature from the ENS	ºC
Solar radiation	srad_ref	Mean daily solar radiation from the REF	MJ m² day^{-1}
	srad_era	Mean daily solar radiation from the ERA5	MJ m² day^{-1}
	srad_ens	Mean daily solar radiation from the ENS	MJ m² day^{-1}
Wind	wnd_ref	2m mean wind speed from the REF	m s^{-1}
	wnd_ era5	2m mean wind speed from the ERA5	m s^{-1}
	wnd_ ens	2m mean wind speed from the ENS	m s^{-1}
Evaporation	et_act	Mean daily actual evapotranspiration from the GLEAM v3	mm day^{-1}
	pet_pm	Mean daily potential evapotranspiration (PM method)	mm day^{-1}
	pet_pt	Mean daily potential evapotranspiration (PT method)	mm day^{-1}
	pet_hg	Mean daily potential evapotranspiration (HG method)	mm day^{-1}
Climate Indices	clim_p	Long-term mean daily precipitation (1980-2010)	mm day^{-1}
	p_seasonality	Seasonality and timing of precipitation (1980-2010)	-
	clim_rh	Long-term mean daily relative humidity (1980-2010)	%
	clim_tmin	Long-term mean daily minimum temperature (1980-2010)	ºC
	clim_tmax	Long-term mean daily maximum temperature (1980-2010)	ºC
	clim_et	Long-term mean daily actual evapotranspiration (1980-2010)	mm day^{-1}
	clim_pet	Long-term mean daily potential evapotranspiration (1980-2010)	mm day^{-1}
	aridity_index	Aridity index (clim_p/clim_pet) of the catchment	-
	clim_srad	Long-term mean daily solar radiation (1980-2010)	MJ m² day^{-1}
	clim_quality	Quality index of climate indices (indicates the source meteorological daily series used for long-term mean calculation)	-

- Means dimensionless

2.3.2 Results and discussion

Figure 4 shows some of the climate attributes for the CABra dataset. Regarding the precipitation derived from our ensemble of Xavier et al. (2016) and ERA5 (Fig. 4a), we found the highest values, reaching up to 10 mm day⁻¹, in the northern portion, and the lowest values, below 1 mm day⁻¹, in the north-eastern portion. Despite the wide range in the daily precipitation, most of the catchments (~80%) presented area-averaged precipitation between 3 and 6 mm day⁻¹.

Figure 4d shows the area-averaged solar radiation reaching the surface, ranging from 10 to 20 MJ m² day⁻¹, with most of the catchments with daily values higher than 15 MJ m² day⁻¹. The spatial distribution of solar radiation is reflected in the temperature values in CABra catchments (Fig. 4e and Fig. 4f). The southern and south-eastern portions present the lowest values of both the maximum and minimum temperatures. This is due to the lower values of solar radiation and high altitudes found in these regions of Brazil. Other areas of Brazil are located in higher latitudes and are subject to higher solar radiation, and due to its flat relief, the temperatures are higher than in the south. Figure 4b indicates that, in most of CABra catchments (~85%), the precipitation seasonal cycle is in timing with the temperature seasonal dynamics, which means that most of the precipitation occurs in the summer (seas > 0). There are only a few catchments in the northern portion of Brazil that have precipitation in the winter (seas < 0), and this can be explained by the high influence of sea breeze on convective precipitation in this region. According to Ahrens (2010) and Kousky et al. (1984), the Amazonian coastal area is highly influenced by the sea breeze, which can occur in 3 out of every 4 days, with the formation of convective activity inland.
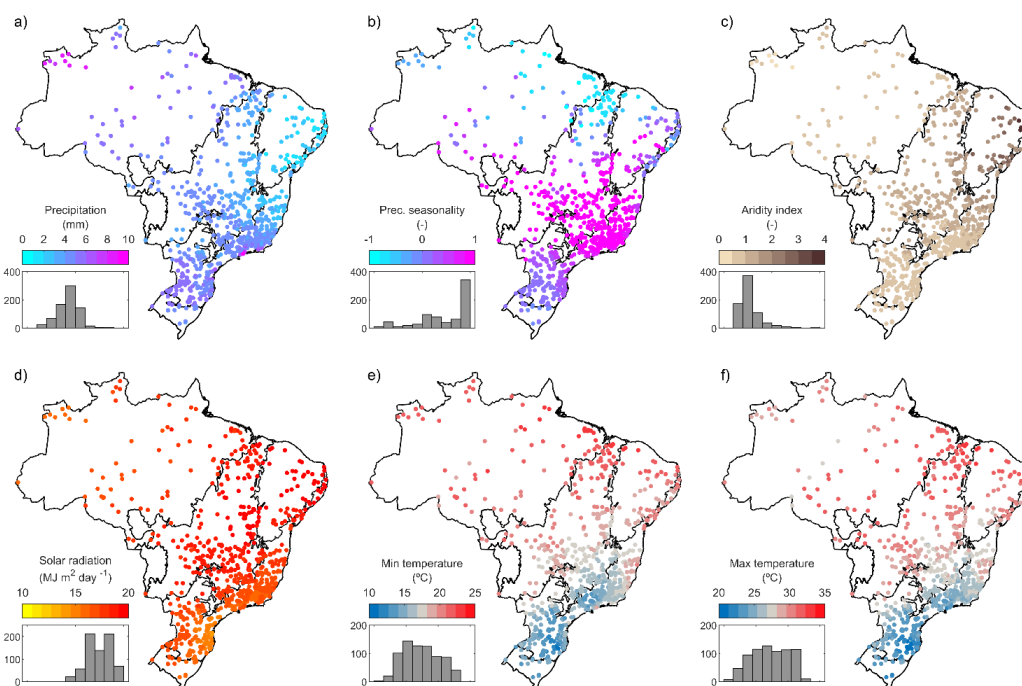
Figure 4: Spatial distribution of climate indices of the CABra catchments. a. Mean daily precipitation, in mm day⁻¹; b. Precipitation seasonality, dimensionless; c. Aridity index, dimensionless; d. Mean daily solar radiation, in MJ m² day⁻¹; e. Mean daily minimum temperature, in ºC; f. Mean daily maximum temperature, in ºC.

250

Our results of the computed potential evapotranspiration are presented in Fig. 5a, Fig. 5b, and Fig. 5c. They are related to three different methods for PET calculation, being: potential evapotranspiration for a reference crop using the Penman-Monteith equation; potential evapotranspiration by the Priestley-Taylor equation; and potential evapotranspiration by the Hargreaves equation. All the equations generated similar results of PET ranging from 3 to 6 mm day^{-1}, with similar spatial

255 variability. The highest values were found for the north-eastern portion of Brazil, with the Penman-Monteith results being slightly higher than other equations. This could be related to the wind component in the method, which is not taken into account in the Priestley-Taylor and Hargreaves methods.
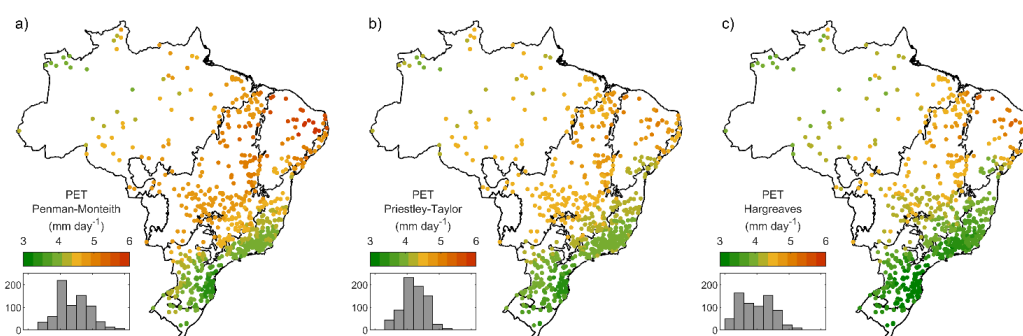
Figure 5: Spatial distribution of the PET calculated from three different methods of the CABra catchments. a. Penman-Monteith
260 **method; b. Priestley and Taylor method; c. Hargreaves method.**

The Budyko framework (Budyko, 1948, 1974) shows that half of CABra catchments are water-limited and the other half are energy limited (Fig. 6). The lowest aridity index values are found in the Amazon and the Atlantic Forest, while the warmer and drier climate can be found in the Cerrado and Caatinga biomes. This may be correlated with the physiognomies of

265 vegetation found in these biomes: tropical forests for the first group and grass and shrub for the second one, and especially, to the water availability and radiation incidence on these abovementioned biomes. Although we have found some outliers which are not explained by the Budyko hypothesis, most of the CABra catchments follow the expected behavior to the long-term mean water balance proposed by Budyko (1948, 1974).
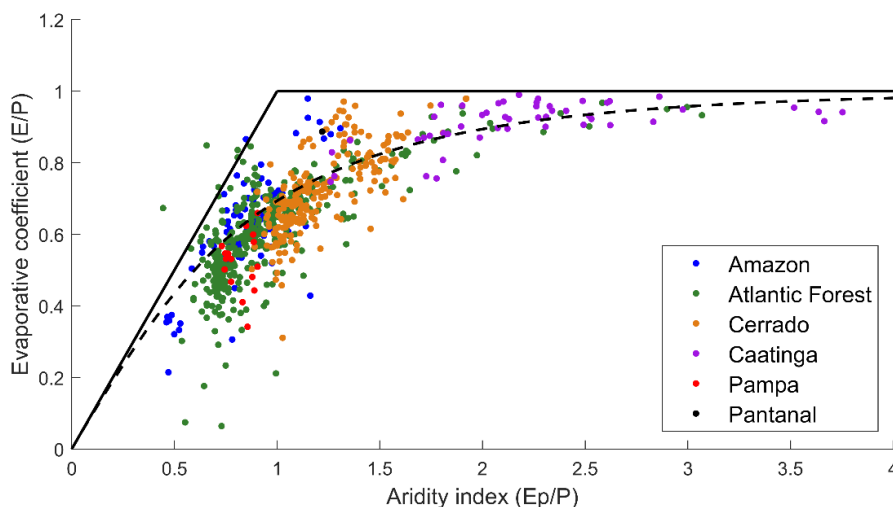
Figure 6: Distribution of the CABra catchments in the Budyko framework. The values of PET and P are from the climate ensemble. Values of E were estimated from the relation P = E + Q, considering long-term means.

2.4 Streamflow and hydrologic signatures

2.4.1 Methodology

The CABra dataset provides daily streamflow records for 735 catchments in Brazil. We used data from streamflow gauges of ANA, where each gauge is related to one of the abovementioned catchments. This dataset is available in the HIDROWEB database (see http://www.snirh.gov.br/hidroweb/). ANA's database contains raw time series of dozens of thousands of gauges of streamflow, precipitation, water quality, and sediment discharge, with a consistency level for each observation. Due to the inconsistencies and missing records in the streamflow data provided by ANA, we implemented filters to take into account only the reliable data for the CABra dataset.

During our analysis, we found four main issues with ANA's database collected from HIDROWEB: (a) missing streamflow values for a period of the time series; (b) duplicate streamflow values with different consistency levels; (c) duplicate values with the same consistency level, and (d) duplicate dates with different values and consistent levels. In the first filter step, we overcame the last three issues by picking up only one of the duplicated values/dates based on the best level of consistency. The first issue is more complex and difficult to overcome as in some cases the missing data reaches almost 100% for some gauges. Since long time series of streamflow is needed for reliable hydrologic investigations, we defined a threshold for the selection of the streamflow gauges considered in the CABra dataset based on the following conditions: at least 30 years of data, comprising the hydrologic years from 1980 to 2010, with up to 10% of missing data. The application of these filters led to 735 streamflow gauges, and consequently, 735 catchments.

After the employment of the filters, we calculated for the 735 selected catchments, a variety of hydrological signatures, which can provide a better understanding of the patterns of functionality and behavior of the catchments. From the quantification of hydrological characteristics, it is possible to explain the variability in responses to climate forcings. We

selected hydrological signatures obtained from widely available hydrological series (see Table 4), as well as Sawicz et al. (2011) e Westerberg e McMillan (2015). A list with more hydrological signatures can be found in Yadav et al. (2007).

295   **Table 4: Hydrological signatures of the CABra dataset.**

Type	Attribute	Long name	Unit
Distribution	q_mean	Mean daily streamflow	mm day^{-1}
	q_1	Streamflow 1st quantile	mm day^{-1}
	q_5	Streamflow 5th quantile	mm day^{-1}
	q_95	Streamflow 95th quantile	mm day^{-1}
	q_99	Streamflow 99th quantile	mm day^{-1}
Frequency and duration	q_hf	Max streamflow frequency	days y^{-1}
	q_hd	Max streamflow duration	days
	q_lf	Min streamflow frequency	days y^{-1}
	q_ld	Min streamflow duration	days
	q_hfd	Half-flow date	day of the year
Dynamics	baseflow_index	Baseflow index	-
	q_cv	Flow coefficient of variation	-
	q_lv	Min flow coefficient of variation	-
	q_hv	Max flow coefficient of variation	-
	q_elasticity	Streamflow elasticity	-
	fdc_slope	The slope of the flow duration curve	-
Runoff	runoff_coef	Runoff ratio	-

- Means dimensionless

2.4.2 Results and discussion

Figure 7 shows the hydrologic signatures calculated for the CABra catchments for the period between the hydrologic years 1980 and 2010. The mean daily flow for the Brazilian catchments ranges from less than 1 mm day^{-1} to up to 9 mm day^{-1},

300   with an overall mean of 2 mm day^{-1}. The highest values were found in the extreme north of Amazon, where the daily flows reached 8 mm day^{-1} due to high amounts of precipitation through the all the year, and in the Atlantic Forest, in the southeast, where we also have steepness relief with higher values of the slope, providing the runoff instead of infiltration process. This can be showed seen in Fig. 7b, related to the runoff coefficient, where we noted the high values in the southern and north-western portions of Brazil. Most of the CABra catchments presented a runoff coefficient up to 0.5 though.

305 Our results also revealed that the Brazilian catchments to be mainly dependent on the baseflow since all of it presented a baseflow index greater than 70%. The lowest values were found in the Caatinga biome, where we also found the lowest mean daily flows. The half-flow date (considering October 1st as the beginning of the hydrologic year) indicates that ~80% of Brazilian catchments reach the half of total accumulated annual flow in less than 200 days (Fig. 7d), showing the high correlation with the seasonal cycle of precipitation. The catchments with later dates of the half-flow day can be found in the

310 Pampa biome, where there is no well-defined rainy/dry season, and in the Amazon, where the amounts of accumulated annual streamflow are too high and the peak of precipitation is near the end of the hydrologic year (Almagro et al., 2020). The analysis of the slope of the flow duration curve, in Fig. 7e, shows the lowest values in a great portion of Brazil, ranging from the Cerrado to the Atlantic Forest and Pampa biomes.

In our analyses, we also found values of the slope of flow duration curve reaching infinity in the north-eastern portion of

315 Brazil, in the Caatinga biome, which indicates the existence of catchments with ephemeral rivers in that region, which are mainly dependent on direct runoff. This can be also seen when analyzing Fig. 7f, related to the streamflow elasticity. The highest values, up to 4, are located in catchments within the same abovementioned region, indicating the strong dependence of those catchments on precipitation events to generate its streamflow. Moreover, we can note that most Brazilian catchments are inelastic to changes in precipitation. This fact can be explained by the high values of the baseflow index,

320 which maintain the streamflow through the year. Fig. 7g, Fig. 7h, and Fig. 7i show the results related to the low flows of CABra catchments.

In general, Brazilian catchments present a low flow (5th quantile) lower than 1 mm day^{-1}, up to 50 days through the year, with a mean duration of up to 25 following days. Despite the mean values, we can note high values (up to 3 mm day^{-1}) in the Amazon. Additionally, higher values of frequency and duration of low flows can be found in the north-eastern portion of

325 Brazil, with mean frequency reaching 150 days and mean duration reaching 100 days for some catchments. In turn, Fig. 7j, Fig. 7k, and Fig. 7l show the information about high flows in CABra catchments. Most CABra catchments present high flows up to 10 mm day^{-1}, but in some catchments, this value can reach 30 mm day^{-1}. As seen in the low flow analyses, the mean frequency of high flow does not exceed 50 days per year for most of the catchments. The frequency, instead, lasts for lower time, up to 10 days. It is important to note the values of frequency and duration of high flows for the Caatinga biome,

330 where the mean streamflow values are too low that the high flow (95th quantile) is easily overcome through the year, leading those catchments to present the highest values of frequency and duration of high flows in Brazil.
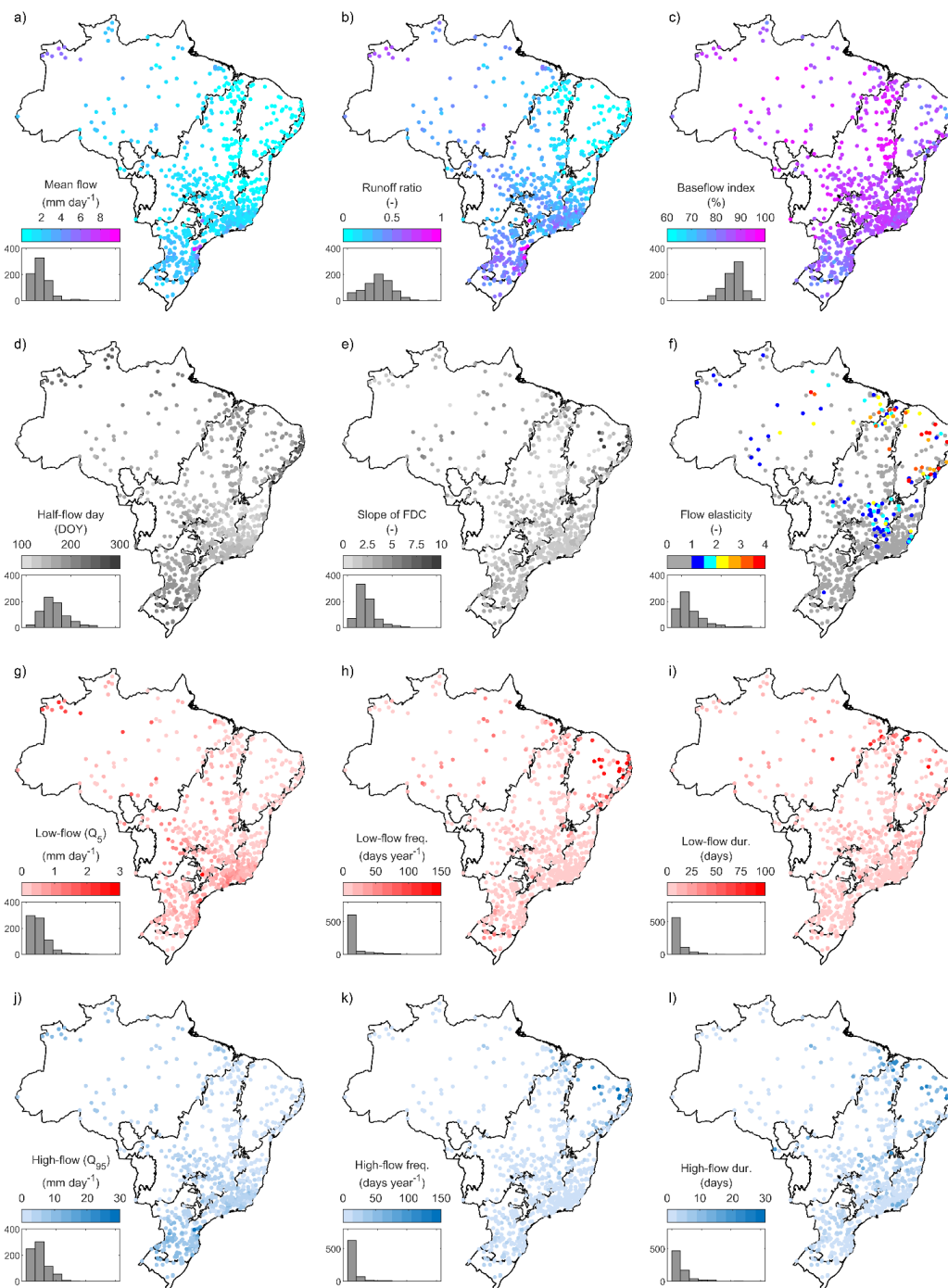
Figure 7: Spatial distribution of the hydrological signatures of the CABra catchments. a. Mean daily streamflow, in mm day⁻¹; b. Runoff ratio, dimensionless; c. Baseflow index, dimensionless; d. half-flow day, in day of the year; e. The slope of the flow duration curve, dimensionless; f. Flow elasticity, dimensionless; g. Low-streamflow, in mm day⁻¹; h. Low-streamflow frequency, in days year⁻¹; i. Low-streamflow duration, in days; j. High-streamflow, in mm day⁻¹; k. High-streamflow frequency, in days year⁻¹; l. High-streamflow duration, in days.

2.5 Groundwater

2.5.1 Methodology

340 The CABra dataset presents four attributes regarding the groundwater at the catchments (Table 5). They are related to the water table (water table depth and height above the nearest drainage) and to the aquifer where the catchment is within (aquifer name and rock type). The first attribute is the area-averaged water table depth. This information was extracted from Fan et al. (2013), which is a global water table depth map generated using a climate-sea-terrain coupled model. The results were validated against observations and show the global patterns of shallow groundwater, making possible the understanding

345 of how groundwater affects terrestrial ecosystems, such as the soil moisture and land hydrology, in a deficiency of rain (Fan et al., 2013; Lo et al., 2010).

The second attribute is the Height Above Nearest the Drainage (HAND), also related to the water table but is an indirect way to infer the water table depth. The HAND is a normalized drainage version of a digital elevation model, where the height is defined as the vertical distance from a hillslope (at the surface cell) to a respective "outlet-to-the-drainage" cell, as defined

350 by Nobre et al. (2011). Considering the local gravitational potential, the HAND model shows robust correlations between soil water conditions and its values. Additionally, the authors created three classes to easily infer about the water table depth (if at the surface, shallow or deep) only using a digital elevation model, which is commonly a piece of difficult and scarce information on a large scale. We also present the aquifer in which the catchment is within (most of the area) and the most common type of rock of the aquifer. This information was provided by the ANA database and it is important to the

355 knowledge of the aquifer geology and its implication to the groundwater storage and recharge.

Table 5: Groundwater attributes of the CABra catchments.

Type	Attribute	Long name	Unit
Water table	catch_wtd	Water table depth	m
Height above nearest drainage	catch_hand	Height above the nearest drainage	m
Aquifers	aquif_name	Aquifer name	-
	aquif_type	Aquifer rock type	-

- Means dimensionless

2.5.2 Results and discussion

360 Our analyses showed a close relationship between the water table depth from Fan et al. (2013) and the HAND. In the northern portion of Brazil, especially in the Amazon, we can find shallow water table depths, while in the south-eastern, especially in the Atlantic Forest, we noted the deepest values for the water table depths (see Fig. 8a and Fig. 8b). This could be related to the altitudes of each catchment since the HAND is a product derived from a digital elevation model. As a

catchment lies at a high elevation, the water table depth is deeper than the other catchments in low elevations. This is
365 particularly noted in the coastal area of the Atlantic Forest, which presents high altitudes and at the same time, is close to the
sea level.

Figure 8c shows that most of the CABra catchments are dominated by fractured and porous rocks. The fractured rocks store
the water in fractures, creating large pockets of water, and due to the nature of the rock, it is hard to drill. The porous rocks
store water in the soil pores (especially in sandy soils originated by sedimentary rocks), and it is common to find large
370 amounts of water in them. Moreover, it is easier to drill than other types, which leads to more exploration of its water. The
two of the world's largest aquifers are in Brazil and are porous, the Guarani Aquifer in the Cerrado biome, and the Alter do
Chão Aquifer in the Amazon biome. The third aquifer type found in CABra catchments is the karstic one. This kind of
aquifer is like the fractured one, but the fractures are much bigger, thereby forming subsurface rivers and lakes. This can be
found in the São Francisco River Basin.
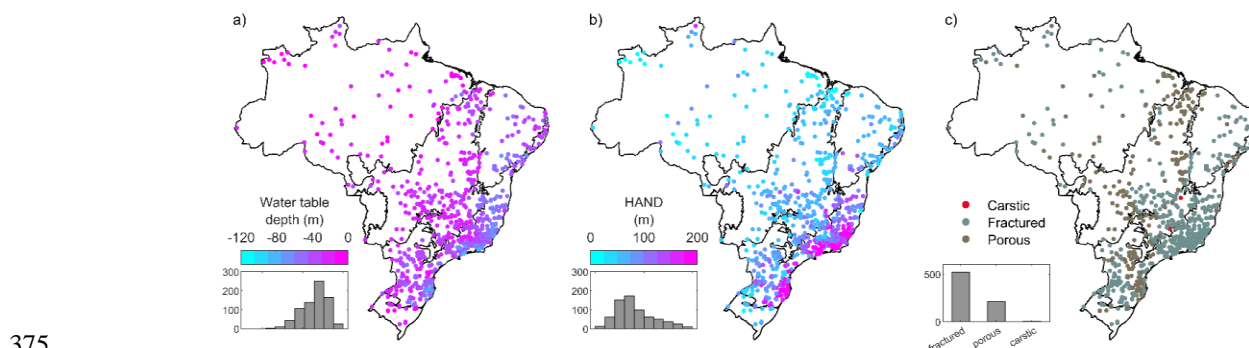
375

Figure 8: Spatial distribution of the groundwater attributes of the CABra catchments. a. Water table depth, in m; b. Height Above Nearest Drainage, in m; c. Type of aquifer bedrock.

2.6 Soil

2.6.1 Methodology

380 The CABra dataset has eight attributes related to the soil type, properties, and texture (Table 6). The soil type of the
catchment presented here is the most common type for each catchment (bigger percentage of the different types) derived
from the Brazilian soil map developed by the Brazilian Agricultural Research Corporation (EMBRAPA, in Portuguese)
(Santos et al., 2011). To meet with the international standards for soil classification, we converted the classes to the widely
used World Reference Base (WRB) (FAO, 2014). Due to the high importance of the knowledge of the soil depth, density,
385 texture, and organic matter to the understanding of soil-water dynamics and root grow (Dexter, 2004; Saxton et al., 1986;
Saxton and Rawls, 2006; Shirazi and Boersma, 1984), we also present the mean areal attributes for them. These fields were
taken from the SoilGrids250m, a global high-resolution gridded soil information based on field measurements, data
assimilation, and machine learning. This is the most detailed and accurate global soil product and is crucial for the
development of large-scale studies in many fields (ecology, climate, hydrology). However, despite all the improvements

390   brought by SoilGrids250m, the data still have limitations, and one of the biggest is the high uncertainty levels for some of its products, such as the depth to bedrock and coarse fragments. Besides, we also employed the United States Department of Agriculture (USDA) soil texture classification, which is a widely used method for soil definition based on the mechanical limits of soil particles. Moreover, previous studies showed that the USDA soil texture classification can potentially reflect other soil parameters and characteristics (Groenendyk et al., 2015; Twarakavi et al., 2010), making it a powerful tool with a

395   low input requirement.

Table 6: Soil attributes of the CABra catchments.

Type	Attribute	Long name	Unit
Soil type	soil_type	Soil type	-
Soil depth	soil_depth	Soil depth to bedrock (m)	m
Soil density	soil_bulkdensity	Soil bulk density	g cm^{-3}
Soil texture	soil_sand	Sand portion on soil (0cm)	%
	soil_silt	Silt portion on soil (0cm)	%
	soil_clay	Clay portion on soil (0cm)	%
	soil_textclass	Soil texture classification (USDA)	-
Organic content	soil_carbon	Soil organic carbon content	‰

- Means dimensionless

2.6.2 Results and discussion

400   The catchments presented 12 main soil classes, with the Ferrasols, Acrisols, and Nitisols being the most common soil types in more than 90% of the CABra catchments (Fig. 9a). The Ferrasols were the dominant soil type in approximately 75% of the catchments, typical of equatorial and tropical regions, which have an advanced stage of weathering of their constitutive material, being normally deep (>1m), well-drained, and acidic soils (high pH levels can occur in areas with a strong dry season, such as observed in the Caatinga biome). Acrisols are formed mainly by minerals, with an evident increase in the

405   clay content from the surface to horizon B, with variable depth and drainage, but always with high acidity. The third most common soil type is the Nitisols, which have a clay texture, with a well-developed B horizon structure, and are usually deep and well-drained with moderate acidity (EMBRAPA, 2018).

We noted that most of the catchments present soil texture dominated by sand and clay (Fig. 9c, Fig. 9d, and Fig. 9e). South-eastern, northern, and central regions of Brazil are dominated by sandy clay loam soils, while the southern portion is

410   dominated by clay, which can reach up to 80%, making this region one of the most productive in terms of agriculture in Brazil. By the employment of the USDA texture triangle, we found 6 classes: clay, clay loam, loam, sandy clay, sandy clay

loam, and sandy loam (see Fig. 9b). The soils presenting a clay and clay loam texture are in the southern portion, especially where the Nitisols occur, which is also the region with a significant portion of the Brazilian agricultural production.

Most of the catchments present a mix of texture, the sandy clay loam, which covers from the south through the central to the

415   northern regions of Brazil. There is a spatial correlation between the soil organic carbon, bulk density, and the distance to the bedrock, as we can see in Fig. 9f, Fig. 9g, and Fig. 9h. In the southern and south-eastern portions, especially in the Atlantic Forest biome, we have a combination of high soil organic carbon, low bulk density, and low distance to the bedrock. These characteristics, allied to the favorable climate, turned this kind of soil attractive to agriculture. On the other hand, other Brazilian regions present the opposite.
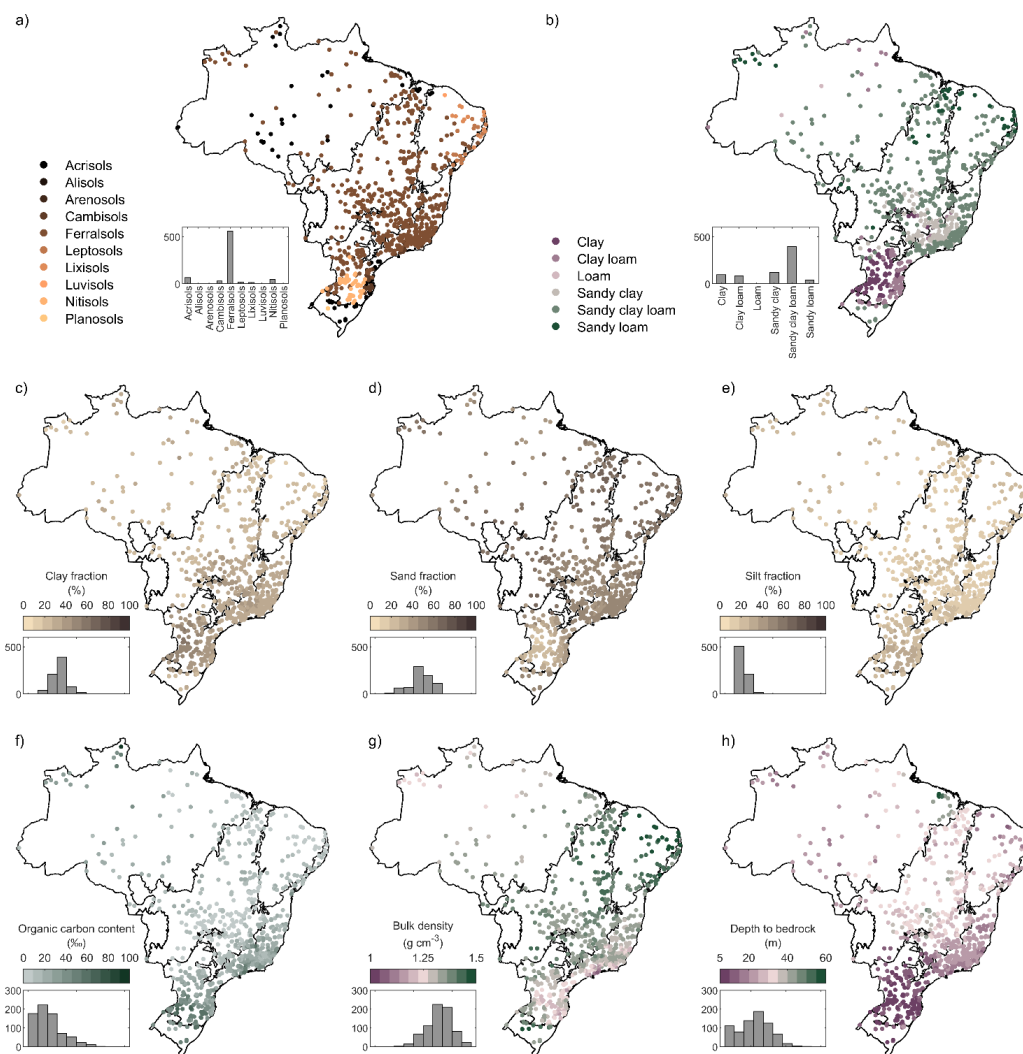
420

Figure 9: Spatial distribution of the soil attributes of the CABra catchments. a. The most common type of soil in the catchment; b. The class of texture based on USDA classification; c. The clay fraction of the soil, in percentage; d. The sand fraction of the soil, in percentage; e. The silt fraction of the soil, in percentage; f. The organic carbon content of the soil, in permille; g. The bulk density of the soil, in g cm⁻³; h. The depth to soil bedrock, in m.

2.7 Geology

2.7.1 Methodology

The CABra dataset presents four attributes related to the geology of the catchments (Table 7), being the predominant lithology class, the subsurface porosity, the subsurface permeability, and the subsurface hydraulic conductivity. The lithology class is derived from the Global Lithologic Map (GLiM) (Hartmann and Moosdorf, 2012). The GLiM is a high-resolution global dataset that describes the geochemical, mineralogical, and physical properties of the rocks in 16 main lithological classes. Moreover, GLiM allows us to better understand the geology of smaller areas, such as our CABra catchments. Also, we are using a GLiM-derivate product of subsurface porosity and permeability named GLobal HYdrogeology MaPS (GLHYMPS), developed by Gleeson et al. (2014). The GLHYMPS is the first large-scale high-resolution mapping of porosity and permeability and fills a lack of robust and spatially distributed subsurface geology map.

The porosity is the void spaces in a material (soil in our case) controls how much fluid (water) can be stored in this material, or in the soil subsurface. The movement of the stored water in the soil is controlled by the permeability, which is the capacity of a porous material (again, soil) to transmit fluids. Both parameters are fundamental to the knowledge of fluid rate and its impacts on Earth's subsurface. When using this kind of high-resolution data for large-scale studies, we can improve our understanding of the dynamics between groundwater and land surface. Considering the saturated hydraulic conductivity as one of the most important physical properties on the quantitative and qualitative assessment of the water movement in the soil, we presented its values in the CABra dataset. Following the assumption that the hydraulic conductivity is separable into the contributions of the porous matrix of the soil, and the density and viscosity of the fluid, we also estimated the hydraulic conductivity of the CABra catchments using its relation to the permeability (Equation 4), as described in Grant (2005).

$$K = \frac{k\rho g}{\mu},$$ (5)

where K is the subsurface hydraulic conductivity, k is the subsurface permeability, ρ is the density of the fluid, g is the gravitational constant (9.8 m s^{-2}), and μ is the viscosity of the fluid. In our study, we have considered the water as the fluid, so we have used ρ = 999.97 kg m^{-3}, and μ = 0.001 kg m^{-1} s^{-1}.

Table 7: Geology attributes of CABra catchments.

Type	Attribute	Long name	Unit
Lithology	catch_lith	Dominant lithology class	-
Subsurface geology	sub_porosity	Subsurface porosity	-
	sub_permeability	Subsurface permeability	m²
	sub_hconduc	Subsurface hydraulic conductivity	m s^{-1}

- Means dimensionless

2.7.2 Results and discussion

Related to the lithology class, the catchments present 10 different classes according to the GLiM dataset: siliciclastic sedimentary rocks, acid volcanic rocks, unconsolidated sediments, acid plutonic rocks, metamorphic rock, mixed sedimentary rocks, basic volcanic rocks, carbonate sedimentary rocks, intermediate volcanic rocks, and pyroclastic rocks
455 (Fig. 10). We found that 35% of the catchments have the metamorphic rocks as the most common lithologic class, a result of continuous weathering on the original rock. These catchments are located especially in the southern portion of Brazil, in mountainous areas. Approximately 39% of CABra catchments are formed by sedimentary rocks, considering its subdivision in siliciclastic, unconsolidated, and mixed resulted from sediment deposition. They are mostly located in flat areas, such as in the Paraná River Basin and São Francisco River Basin, in the central and north-eastern portion of Brazil. 25% of catchments
460 presents igneous rocks (plutonic and volcanic) as the most common lithology class, resulted from volcanic eruptions. These catchments are located mainly in the Atlantic Forest biome, although we can find some catchments in the Amazon.

In respect to the subsurface, most CABra catchments presented values lower than 20%, with a mean value of 10%. Catchments in the Atlantic Forest presented the lowest values of the catchments set. Results regarding the subsurface permeability and hydraulic conductivity reinforce the heterogeneity and random occurrence of these soil properties. As we
465 can see in Fig. 10c and Fig. 10d, there is no well-defined spatial behavior for them. Subsurface permeability ranges from -14 to -12 m² in log scale, with a mean of -13.4 m², while the subsurface hydraulic conductivity presented a mean value of -6.4 m s^{-1} in log scale, vary between -10 to -4 m s^{-1} in log scale.
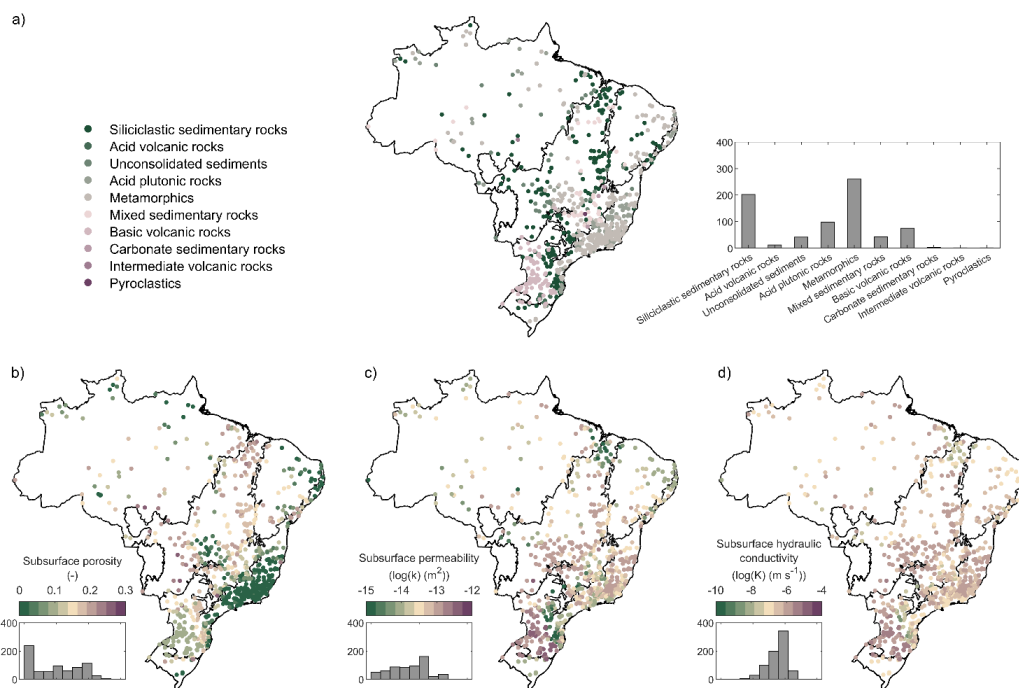
Figure 10: Spatial distribution of geology attributes of the CABra catchments. a. Most common lithology class in the catchment; b.
470 **Subsurface porosity, dimensionless; c. Subsurface permeability, in m²; d. Subsurface hydraulic conductivity, in m s^{-1}.**

2.8 Land-cover

2.8.1 Methodology

The CABra dataset presents 14 attributes regarding the land-cover and land-use of the Brazilian catchments (Table 8). They are related to the area-averaged land-cover and land-use itself (dominant cover type, and the cover fractions of 9 main

475   classes of use: bare soil, forest, grass, shrub, moss, crops, urban, snow, and water) and to the area-averaged intra-annual variability of the vegetation biomass, here represented by the Normalized Difference Vegetation Index. The land-cover and land-use map used in the CABra dataset is the Copernicus Global Land Cover, which has 100-m spatial resolution, is a result of a classification of the PROBA-V satellite observations of the year 2015 and follows the UN FAO Land Cover Classification System (Buchhorn et al., 2019) available at https://land.copernicus.eu/global/lcviewer.

480   As an indicator for the vegetation biomass of the land-cover through the year, we are using the seasonal NDVI for each CABra catchment, derived from the Long Term Statistics (LTS) based on the Normalized Difference Vegetation Index (NDVI) from the Copernicus Global Land services. This dataset is an NDVI mean for each month of the year during the 1999-2017 period, obtained from the SPOT-VGT and PROBA-V sensors in a 1-km spatial resolution, available at https://land.copernicus.eu/global/products/ndvi. The NDVI is obtained by calculating the spectral reflectance difference

485   between red and near-infrared bands of the satellite image (Tucker, 1979) (Equation 5) and ranges from -1 to +1, with the highest values attributed to areas with greater vegetation cover.

$$\text{NDVI} = \left(\frac{\text{NIR}-\text{RED}}{\text{NIR}+\text{RED}}\right), \tag{4}$$

where NIR is the surface spectral reflectance in the near-infrared band and RED is the surface spectral reflectance in the red band.

490

Table 8: Land-cover attributes of CABra catchments.

Type	Attribute	Long name	Unit
Land-cover **and** **land-use**	cover_main	Dominant cover type	-
	cover_bare	Bare soil fraction of cover	%
	cover_forest	Forest fraction of cover	%
	cover_grass	Grass fraction of cover	%
	cover_shrub	Shrub fraction of cover	%
	cover_moss	Moss fraction of cover	%
	cover_crops	Crops fraction of cover	%
	cover_urban	Urban fraction of cover	%
	cover_snow	Snow fraction of cover	%
	cover_water	Water fraction of cover	%
Vegetation	ndvi_djf	DJF normalized difference vegetation index	-
	ndvi_mam	MAM normalized difference vegetation index	-
	ndvi_jja	JJA normalized difference vegetation index	-
	ndvi_son	SON normalized difference vegetation index	-

- Means dimensionless

2.8.2 Results and discussion

We observed that most of the Brazilian catchments are covered by forest and grass (Fig. 11). The shrub is the dominant cover for most of Caatinga catchments, while the grass is the dominant one in the Cerrado (tropical savannah). The forest cover is dominant especially in the Amazon and Atlantic Forest, as these two biomes are known by tropical forest occurrence, but even though the forest cover is not the most common for all the CABra catchments, ~85% of them present at least 20% of it (Fig. 11b). The grass cover fraction presented values up to 40% of the area for most of the catchments but reached 60% in some cases (Fig. 11c). The highest values were found in the Cerrado and Atlantic Forest biomes, in central and south-eastern portions of Brazil.

Large areas of natural cover were converted to agricultural lands (including crops and pasture) in past years (Gibbs et al., 2010, 2014), and satellite sensors and classifiers algorithms cannot separate natural grassland and pasture/managed grasslands, as described in the PROBA-V documentation. Figure 11d gives us a better idea of this. Probably the fraction of the shrub cover of the Cerrado is the natural cover remaining for this biome since this is the expected type of vegetation. As seen in Fig. 11e, a few numbers of catchments present the crops as the dominant cover type, mostly in the central and

southern region, but we can also see the great fraction of crop cover in the MATOPIBA region, one of the largest agriculture frontiers in Brazil (Gibbs et al., 2014; Pires et al., 2016; Spera et al., 2016). Figure 11f shows that there are only a few cases of urban catchments, within or close to major Brazilian cities that present this type of cover, showing that the CABra dataset is mainly composed of either natural or minimally (hydrologically) modified catchments.
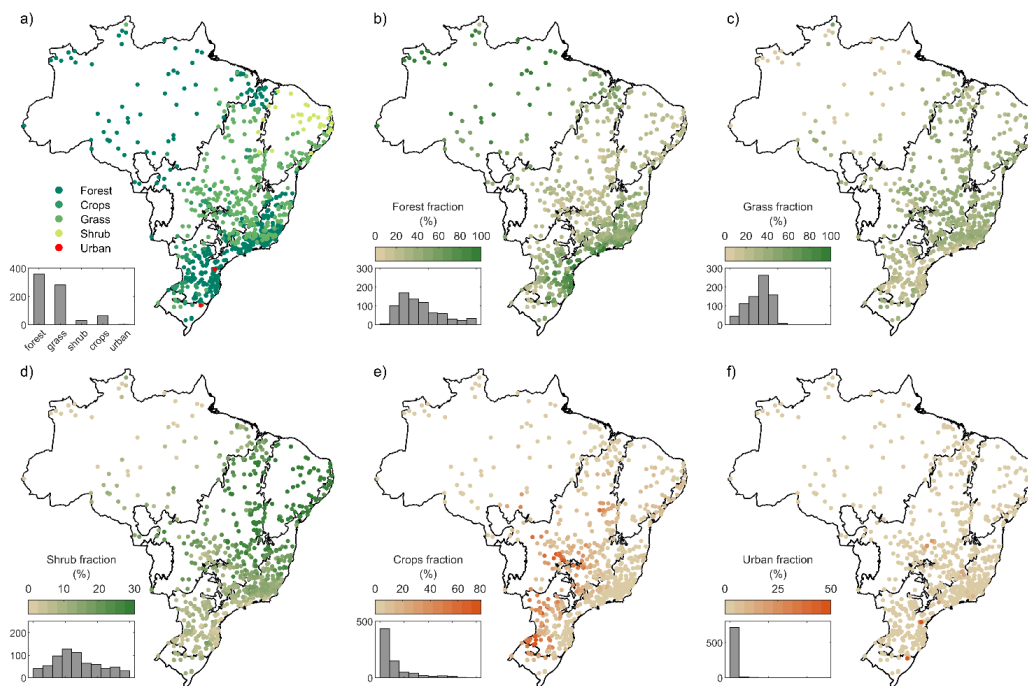
Figure 11: Spatial distribution of the land-cover and land-use attributes of the CABra catchments. a. The most common land-cover type in the catchment; b. Forest fraction of land-cover, in percentage; c. Grass fraction of land-cover, in percentage; d. Shrub fraction of land-cover, in percentage; e. Crops fraction of land-cover, in percentage; f. Urban fraction of land-cover, in percentage.

The seasonal variability of the NDVI can be seen in Fig. 12. Although the mean seasonal values for the entire country are similar (0.65 for DJF, 0.69 for MAM, 0.64 for JJA, and 0.56 for SON), the spatial variability of the NDVI values are noticeable. There is a clear relationship with the annual cycle of precipitation, and that is why it is so important to consider the seasons to analyze the NDVI. Higher values were found in timing with the precipitation cycle in all the biomes, in DJF and MAM months. Even in the Amazon, we can see a considerable decrease in the NDVI values for the catchments in the dry seasons (JJA and SON) as well as the other biomes and regions of Brazil. NDVI reaches the lowest values at the end of the hydrological year and then starts to increase the values only at the beginning of the rainy season, i.e., DJF season. Intermediate values in the central portion of Brazil are much likely to be linked to agricultural production, leading the values to be lower than the natural cover.
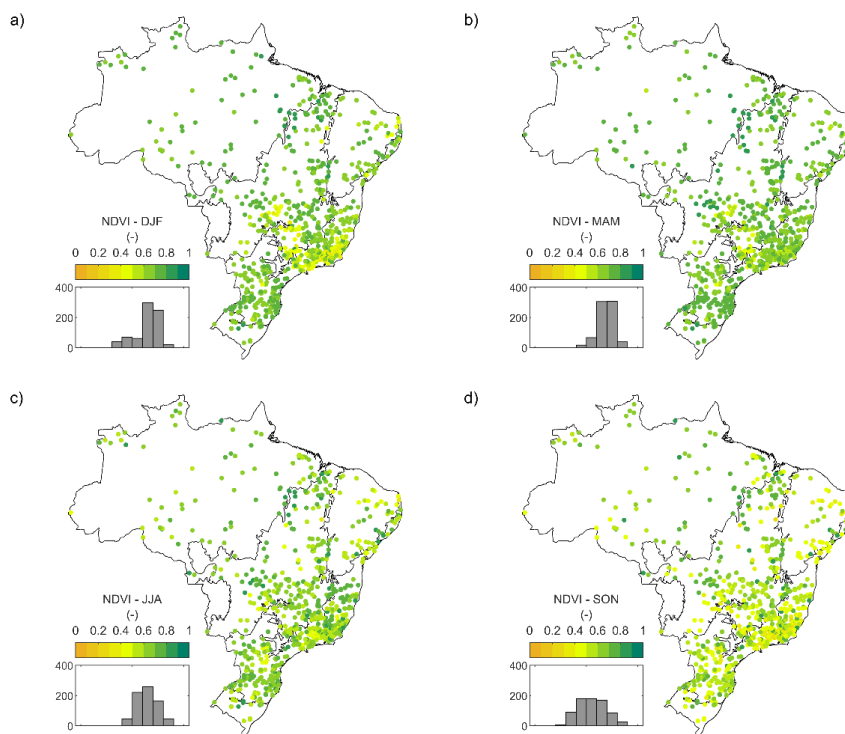
Figure 12: Spatial distribution of the seasonal NDVI of the CABra catchments. a. NDVI in summer season (DJF); b. NDVI in autumn season (MAM); c. NDVI in the winter season (JJA); d. NDVI in the spring season (SON).

530

2.9 Hydrologic disturbance

2.9.1 Methodology

The CABra dataset presents 6 attributes related to the hydrologic disturbances on catchments water fluxes (Table 9). Anthropic changes in water flux patterns, which happens outside the range of natural flow and climate extremes, can directly

535   impact the water availability and quality, stream channel geometry and sedimentation, and the equilibrium of ecosystems (Boulton et al., 1992; Coleman et al., 2011; Whited et al., 2007). Natural conditions of catchments are constantly modified by human interactions such as land-cover and land-use changes, flow regulation, water abstractions, soil impermeabilization, and many others, which can drastically alter the way hydrologic fluxes in the catchments respond.

Considering the relevance of the abovementioned human interactions, we provided information about the number and

540   volume of the reservoirs (which can regulate streamflow), water demand extracted from ANA (2017), and using some of the CABra attributes, we have created a hydrologic disturbance index, which will easily provide for CABra users the degree of human interactions that can modify water fluxes in each catchment. In the development of this index, we have considered fraction of urban cover in each catchment, the distance to the nearest urban area of each catchment, the number of reservoirs

in each catchment, the total volume of reservoirs in each catchment, and its flow regulation capacity, the fraction of reservoir
545 area of each catchment area, and the annual water demand. The equation related to the hydrologic disturbance index can be
found in the following Equation 6:

$$HD_{index} = 0.4([U_C . U_D] + CR_C) + 0.05R_N + 0.05R_{\%A} + 0.4R_R + 0.1W_D, \tag{6}$$

where HD_{index} is the hydrologic disturbance index, dimensionless; U_C is the normalized fraction of urban cover; U_D is the
normalized distance to the nearest urban area; CR_C is the normalized fraction of crops cover; R_N is the normalized number of
550 reservoirs; $R_{\%A}$ is the normalized percentage of catchment's area covered by reservoirs; R_R is the normalized reservoirs'
regulation capacity of catchment's mean annual flow; and W_D is the normalized catchment's annual water demand.

Table 9: Hydrologic disturbance attributes of CABra catchments.

Type	Attribute	Long name	Unit
Reservoirs	res_number	Number of catchment's reservoirs	-
	res_area	The total area of catchment's reservoirs	km²
	res_area_%	Catchment's area percentage covered by reservoirs	%
	res_volume	The total volume of catchment's reservoirs	hm³
	res_regulation	Reservoir's regulation capacity of the mean annual flow	-
Water demand	water_demand	Water demand in the catchment	mm year^{-1}
Land-cover	cover_urban	Urban fraction of cover	%
	cover_crops	Crops fraction of cover	%
	dist_urban	Distance from gauge to nearest urban cover	km
Hydrologic disturbance index	hdisturb_index	Index of hydrologic disturbance in the catchment	-

- Means dimensionless

2.9.2 Results and discussion

555

The results of the spatial distribution of the hydrological disturbance index and its components are shown in Fig. 13. Most
CABra catchments are close to an urban cover (it can be a large city or a small village), with a distance of up to 10 km.
However, we also could find catchments with up to 100 km of distance to the urban cover. As seen in Fig. 13b and Fig. 13c,
most CABra catchments present a fraction of urban cover up to 10%, with high values close to large cities, and a fraction of
560 crops cover up to 40%, with the highest values in central and southern portions. As these factors present a high weight on the
hydrological disturbance index, they are a good clue of the most disturbed catchments.

Results from the reservoirs in CABra catchments are shown in Fig. 13d, Fig. 13e, Fig. 13f, and Fig. 13g. The number of reservoirs in the catchment ranges from zero to 48,404. Even though we found the largest number of reservoirs in a large catchment, this relationship is not linear. There are some catchments, especially in the São Francisco River Basin, which
565 presents an extremely high number of reservoirs due to the low amounts of annual precipitation and intensive drought in the region. Moreover, catchments in the São Francisco River Basin presents the highest values of the total volume of reservoirs. These reservoirs are used for many anthropogenic purposes, such as hydroelectric power plants, irrigation, drinking water supply, fish-farming, and recreation. These high values of the total volume of reservoirs, especially in the drier regions, could lead to a strong streamflow regulation, as seen in Fig. 13g. In most of the CABra catchments, reservoirs can regulate
570 up to 25% of the annual flow, but there are some cases in the Caatinga biome where the regulation capacity reaches up to ten times the annual flow, making these catchments susceptible to non-natural events.

The water demand on CABra catchments ranges from zero (in Amazon) to 171 mm year^{-1} (in Caatinga) and it is related to drinking water supply and irrigation of agricultural areas (Fig. 13h). The integrated analysis of the above-mentioned attributes is shown in Fig. 13i, as the new hydrological disturbance index. Most of the CABra catchments present an index
575 value of up to 0.2, indicating a low anthropic interference on water fluxes. Higher values, above 0.4, indicate catchments with some significant interference on water fluxes, which may be related to one or more terms of the equation. High values of the hydrological disturbance index in the central and southern portion of Brazil may be related to agriculture development, while in the south-eastern part, they may be related to urbanization, and in the north-eastern part, they may be related to the presence of numerous voluminous reservoirs. As expected, in the Amazon and mountainous areas of Atlantic Forest, low
580 values were found. The creation of the hydrological disturbance index can be especially useful for the users of the CABra dataset, allowing them to quickly view the general state of the anthropogenic interferences on water fluxes, which is an important consideration in a wide range of studies.
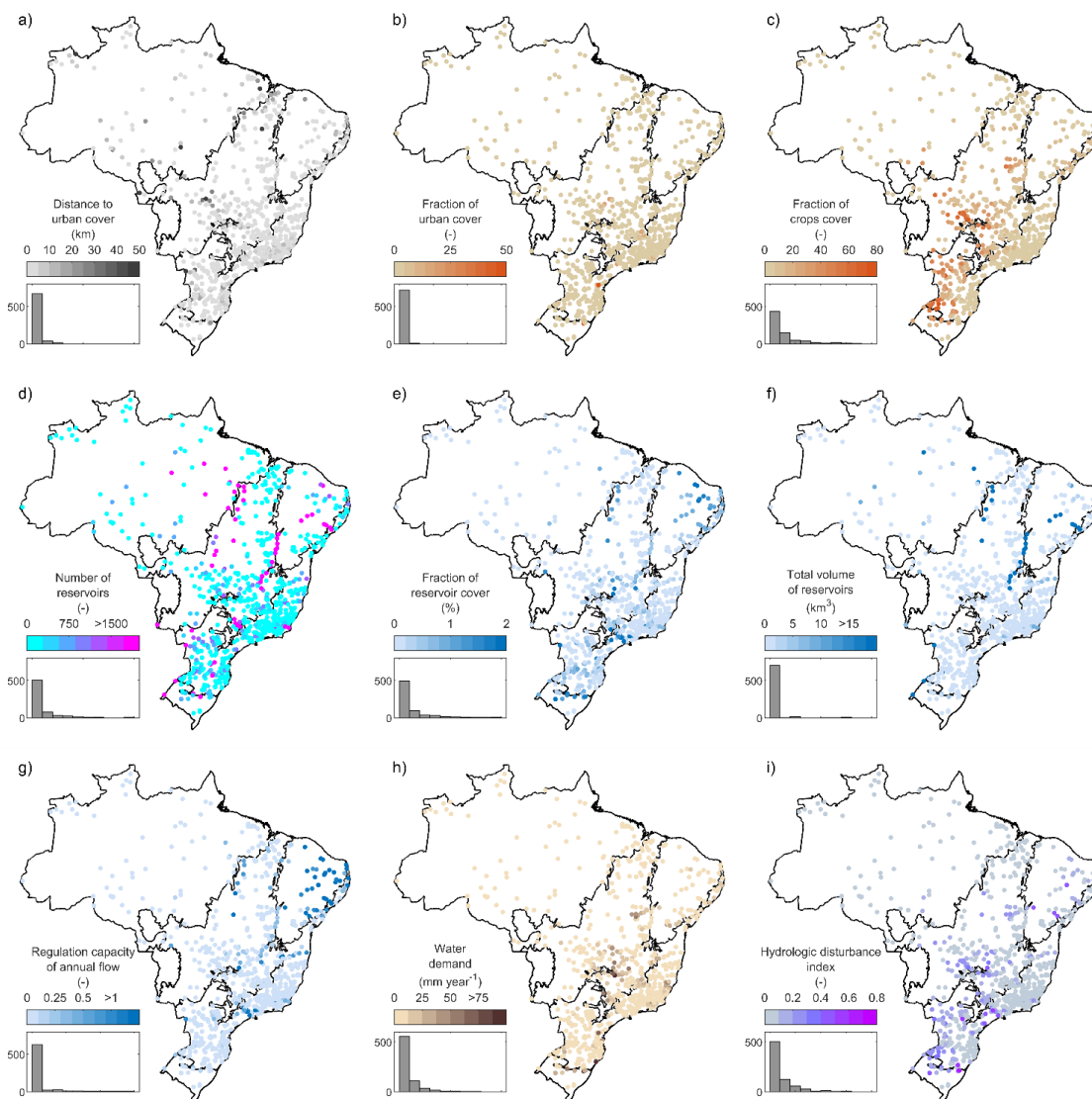
Figure 13: Spatial distribution of the hydrologic disturbance attributes of CABra catchments. a. Distance from urban cover to the
585 **streamflow gauge, in km; b. Urban fraction of land-cover, in percentage; c. Crops fraction of land-cover, in percentage; d. The number of reservoirs in the catchment; e. Reservoir fraction of land-cover, in percentage; f. The total volume of the reservoirs in the catchment, in km³; g. The capacity of the reservoirs in the catchment to regulate the mean annual streamflow, dimensionless; h. Multi-purpose water demand in the catchment, in mm year⁻¹; i. Hydrologic disturbance index (HDI) of the catchment, dimensionless. The HDI is a weighted relationship between all the anthropogenic factors of the catchments.**

590

3 Comparison with the CAMELS-BR and broader implications for hydrological studies

The CABra and the CAMELS-BR (Chagas et al., 2020) contain both large samples of hydroclimatic, landscape, and other attributes for Brazilian catchments. Their striking similarities in concept and goals highlight nothing but the urgent need for the creation of such a database for Brazilian catchments. However, it is important to notice that multiple differences between
595   both datasets exist, as we will discuss below.

The first main difference between CABra and CAMELS-BR is related to the catchment delineation procedures adopted. CAMELS-BR uses the basin masks from the GSIM (Do et al., 2018) product, where a 500-m digital elevation model was used for the delineation of catchment boundaries and extraction of topographic indices. GSIM has a quality filter allowing for up to 50% of error in the catchment area when compared with ANA's value, as described in Do et al. (2018). As
600   previously explained, the CABra catchment boundaries (delineated using streamflow gauge location from ANA), uses a high-definition (90-m) elevation product. We have manually inspected each of the 735 catchments to minimize further errors, correcting the geographic position of the outlet to coincide with the stream network, achieving a mean error of 2% against ANA's areas. It is important to highlight that a suitable watershed delineation is of paramount importance for catchment hydrology studies because errors in these processes are further propagated for all computed attributes dependents
605   on area and location.

Related to the daily streamflow data, in the CABra dataset we have retained catchments with less than 10% missing streamflow records over 30 hydrologic years (1980-2010) which resulted in the final selection of 735 catchments. On the other hand, CAMELS-BR contains 897 catchments with less than 5% missing data, while considering 20 hydrologic years, (1990-2009). Our choice for a longer time series was predicated on the commonly adopted rationale which assumes 30 years
610   as the basis for establishing long-term climatology as well as hydrologic indices (Huntingford et al., 2014; Tetzlaff et al., 2017), which we in turn believe will lead to better characterization of hydrological and climatological processes taking place. Another important difference between both datasets is related to the choice of databases used for providing the daily meteorological time series and estimated the related indices. While CAMELS-BR uses three widely used gridded datasets (based on remote sensing/reanalysis/gauge blends of rainfall), i.e., the CHIRPS v2.0, CPC, and MSWEP v2.2, being the first
615   one the chosen for the climatic indices (because of its spatial resolution of 0.05ºx0.05º), the CABra uses the Xavier et al. (2016) dataset and the ERA5 reanalysis. The Xavier et al. (2016) dataset was produced based on observations from 3,625 rain gauges and 735 wheatear stations in the Brazilian territory and is extensively used as the ground-truth reference for the validation of precipitation products, including the CHIRPS, MSWEP, and the soil moisture satellite-corrected estimates (SM2RAIN, Brocca et al. (2014)) (Paredes-Trejo et al., 2018), the Global Precipitation Measurement (GPM, Hou et al.
620   (2014)) (Gadelha et al., 2019), the Tropical Rainfall Measuring Mission (TRMM, Huffman et al. (2007)) (Melo et al., 2015). Other uses of this dataset include the evaluation of precipitation from downscaled-global circulation models (Almagro et al., 2020), as well as other meteorological variables used in regional studies (Battisti et al., 2019; Bender and Sentelhas, 2018;

Monteiro et al., 2018), aside from being widely used for hydrological studies (Almagro et al., 2017; Avila-Diaz et al., 2020; Lima and AghaKouchak, 2017; Souza et al., 2016).

625 Additional differences belonging to the meteorological time-series section are also worth noting. CAMELS-BR provides the model-based PET estimates extracted from the GLEAM product (Martens et al., 2017), while daily temperatures (maximum, minimum, and average) are the only PET-related variable provided in a daily time series format. The CABra dataset provides the computed PET following 3 widely used methods, along with all necessary variables for its computation, such as solar radiation, wind speed, temperature, and relative humidity. Our choice for the computation of PET instead of using model-

630 based estimates should allow for more transparency and reproducibility of results obtained using our dataset. Also, the choice of providing a wider range of meteorological variables allows the user to estimate PET based on different methods while enhancing the reach of our dataset for studies that might benefit from additional meteorological variables.

While the soil and geology attributes of from both CABra and CAMELS-BR are derived from the same data sources, (i.e., the SoilGrids250, the GLiM, and the GLHYMPS v2.0), CABra provides the following additional variables not available in

635 CAMELS-BR: subsurface permeability (subsurface hydraulic conductivity for geology attribute), soil type, textural class, and soil bulk density – which can be used to estimate soil porosity. Regarding groundwater attributes, CABra contains rock type and name of the aquifer and water table depths from Fan et al., (2013) and the HAND estimates, while CAMELS-BR contains only the water table depth estimates from Fan et al., (2013).

In terms of land-cover attributes, CABra and CAMELS-BR present similar attributes, but the data source is different. CABra

640 adopted a product with a higher spatial resolution (100-m against 300-m) and more recent observation (2015 against 2009) than in CAMELS-BR. Due to this better spatial resolution. we chose to use a most recent land cover, even it being outside of the timespan of hydrologic time series. CABra also brings information about the seasonal vegetation biomass of the catchment, in terms of NDVI, which is not present in CAMELS-BR.

Finally, both datasets take into account the human influence within each catchment, which is essential to a holistic

645 understanding of the catchment behavior due to anthropogenic interactions and a lack of most of the large-sample datasets (Addor et al., 2020). CAMELS-BR presents data about water use, the volume of reservoirs, and the degree of regulation of the reservoirs. However, there is no combination or integration of these attributes in a specific index or approach. On the other hand, CABra presents eight attributes, i.e., distance to urbanization, the fraction of non-natural land-cover (crops and urban areas), water demand, reservoirs' count, area, volume, and streamflow regulation capacity (the last two are also found

650 in CAMELS-BR), which can affect the hydrologic behavior of the catchment in terms of water quantity, quality and regulation. Additionally, we developed a new hydrologic disturbance index (HDI), which considers all these eight attributes above-mentioned. The HDI is a quantitative index of the level of anthropization, being reproducible and practical to identify a more or less human-impacted catchment.

4 Conclusions

655 In this study, we have collected, synthesized, organized, and made available more than 100 topography, climate, streamflow, groundwater, soil, geology, land-use, and land cover, and hydrologic disturbance attributes for 735 catchments in Brazil. To do so, we have used several sources, such as observed time series, observed and modeled gridded data, remote sensing data, and reanalysis data. Moreover, we have calculated some attributes for providing more accurate data than those available in the literature, including potential evapotranspiration, and providing inexistent data, such as the hydrological disturbance

660 index. As this dataset deals with catchment-scale averaged attributes, we have paid particular attention to DEM resolution, catchment delineation, while also manually inspecting each of the CABra catchments.

The development of the CABra dataset opens up several opportunities to test and develop a hypothesis in a unique environment like Brazil, with its vast and rich diversity in hydrology and landscapes. Finding relationships between the catchments' attributes will enable hydrologists to identify the drivers of the water fluxes in the catchment. We hope our

665 dataset will aid catchment classification efforts that will ultimately unravel the underlying dominant controls of Brazilian regional hydrology across space and time. At the same time, the CABra dataset covers fundamentally different hydroclimatologic and ecologic regions than those covered by other similar large-sample datasets (United States, Great Britain, Chile, etc.), being a complement for global assessments and expanding the possibility of the use of our dataset for multiple scientific areas, such as geology, agronomy, ecohydrology.

670 We intend to expand the CABra dataset in the future. Information and attributes related to relevant fields of work, such as soil erosion, ecology, biology, and chemistry, as well as climate change projections, will be added to the CABra dataset in future updates release. Thus, CABra represents a robust multi-source data collection effort for Brazil and is intended to play a key role in advancing the scientific understanding of climate-landscape-hydrology interactions. As such, we hope it will guide large-sample hydrology investigations and pave the way for testing novel hypotheses by both the Brazilian and the

675 international scientific community.

Data availability

The datasets underlying the CABra dataset are available at https://doi.org/10.5281/zenodo.4070147.

Author contribution

680 AA, PTSO, AAMN, and PT conceived the ideas and designed the methodology for the study; AA collected, processed, and analyzed the data; AA, PTSO, and AAMN led the writing of the initial draft; TR and PT edited and reviewed the manuscript; All authors contributed and gave final approval for publication.

Competing interests

685   The authors declare that they have no conflict of interest.

Acknowledgments

This study was supported by grants from the Ministry of Science, Technology, and Innovation – MCTI and National Council for Scientific and Technological Development – CNPq [grants numbers 441289/2017-7 and 306830/2017-5]. This study was also financed in part by the Coordenação de Aperfeiçoamento de Pessoal de Nível Superior - Brasil (CAPES) - Finance
690   Code 001 and CAPES Print.

References

Abramowitz, G., Herger, N., Gutmann, E., Hammerling, D., Knutti, R., Leduc, M., Lorenz, R., Pincus, R. and Schmidt, G. A.: Model dependence in multi-model climate ensembles: weighting, sub-selection and out-of-sample testing, Earth Syst. Dyn. Discuss., 6, 1–20, doi:10.5194/esd-2018-51, 2018.

695   Addor, N., Newman, A. J., Mizukami, N. and Clark, M. P.: The CAMELS data set: catchment attributes and meteorology for large-sample studies, Hydrol. Earth Syst. Sci., 21, 5293–5313, doi:10.5194/hess-21-5293-2017, 2017.

Addor, N., Do, H. X., Alvarez-Garreton, C., Coxon, G., Fowler, K. and Mendoza, P. A.: Large-sample hydrology: recent progress, guidelines for new datasets and grand challenges, Hydrol. Sci. J., 65(5), 712–725, doi:10.1080/02626667.2019.1683182, 2020.

700   Ahrens, C. D.: Essentials of Meteorology: an invitation to the atmosphere., 2010.

Allen, R. G., Pereira, L. S., Raes, D. and Smith, M.: FAO Irrigation and Drainage Paper No. 56 - Crop Evapotranspiration., 1998.

Almagro, A., Oliveira, P. T. S., Nearing, M. A. and Hagemann, S.: Projected climate change impacts in rainfall erosivity over Brazil, Sci. Rep., 7(8130), 1–12, doi:10.1038/s41598-017-08298-y, 2017.

705   Almagro, A., Oliveira, P. T. S., Rosolem, R. and Hagemann, S.: Performance evaluation of Eta/HadGEM2-ES and Eta/MIROC5 precipitation simulations over Brazil, Atmos. Res., 244(1 November 2020), 105053, 2020.

ANA: Conjuntura dos recursos hídricos no Brasil 2019: informe anual / Agência Nacional de Águas., 2019.

Ao, T., Ishidaira, H., Takeuchi, K., Kiem, A. S., Yoshitari, J., Fukami, K. and Magome, J.: Relating BTOPMC model parameters to physical features of MOPEX basins, J. Hydrol., 320(1–2), 84–102, doi:10.1016/j.jhydrol.2005.07.006, 2006.

710   Avila-Diaz, A., Benezoli, V., Justino, F., Torres, R. and Wilson, A.: Assessing current and future trends of climate extremes across Brazil based on reanalyses and earth system model projections, Clim. Dyn., 55(5–6), 1403–1426, doi:10.1007/s00382-020-05333-z, 2020.

Battisti, R., Bender, F. D. and Sentelhas, P. C.: Assessment of different gridded weather data for soybean yield simulations

in Brazil, Theor. Appl. Climatol., 135(1–2), 237–247, doi:10.1007/s00704-018-2383-y, 2019.

715   Bender, F. D. and Sentelhas, P. C.: Solar radiation models and gridded databases to fill gaps in weather series and to project climate change in Brazil, Adv. Meteorol., 2018, doi:10.1155/2018/6204382, 2018.

Berghuijs, W. R., Larsen, J. R., van Emmerik, T. H. M. and Woods, R. A.: A Global Assessment of Runoff Sensitivity to Changes in Precipitation, Potential Evaporation, and Other Factors, Water Resour. Res., 53(10), 8475–8486, doi:10.1002/2017WR021593, 2017.

720   Beven, K., Asadullah, A., Bates, P., Blyth, E., Chappell, N., Child, S., Cloke, H., Dadson, S., Everard, N., Fowler, H. J., Freer, J., Hannah, D. M., Heppell, K., Holden, J., Lamb, R., Lewis, H., Morgan, G., Parry, L. and Wagener, T.: Developing observational methods to drive future hydrological science: Can we make a start as a community?, Hydrol. Process., 34(3), 868–873, doi:10.1002/hyp.13622, 2020.

Boulton, A. J., Peterson, C. G., Grimm, N. B. and Fisher, S. G.: Stability of an aquatic macroinvertebrate community in a

725   multiyear hydrologic disturbance regime, Ecology, 73(6), 2192–2207, doi:10.2307/1941467, 1992.

Brocca, L., Ciabatta, L., Massari, C., Moramarco, T., Hahn, S., Hasenauer, S., Kidd, R., Dorigo, W., Wagner, W. and Levizzani, V.: Soil as a natural rain gauge: Estimating global rainfall from satellite soil moisture data, J. Geophys. Res. Atmos., 119(9), 5128–5141, doi:10.1002/2014JD021489, 2014.

Buchhorn, M., Smets, B., Bertels, L., Lesiv, M., Tsendbazar, N.-E., Herold, M. and Fritz, S.: Copernicus Global Land

730   Service: Land Cover 100m: epoch 2015: Globe, , doi:10.5281/ZENODO.3243509, 2019.

Budyko, M. I.: Evaporation under natural conditions, Israel Program for Scientific Translations, Jerusalem., 1948.

Budyko, M. I.: Climate and Life, Elsevier, New York., 1974.

Chagas, V. B. P., Chaffe, P. L. B., Addor, N., Fan, F. M., Fleischmann, A. S., Paiva, R. C. D. and Siqueira, V. A.: CAMELS-BR: hydrometeorological time series and landscape attributes for 897 catchments in Brazil, Earth Syst. Sci. Data,

735   12(3), 2075–2096, doi:10.5194/essd-12-2075-2020, 2020.

Coleman, J. C., Miller, M. C. and Mink, F. L.: Hydrologic disturbance reduces biological integrity in urban streams, Environ. Monit. Assess., 172(1–4), 663–687, doi:10.1007/s10661-010-1363-1, 2011.

Dexter, A. R.: Soil physical quality Part I. Theory, effects of soil texture, density, and organic matter, and effects on root growth, Geoderma, 120(3–4), 201–2014, doi:10.1016/j.geodermaa.2003.09.005, 2004.

740   Do, H. X., Gudmundsson, L., Leonard, M. and Westra, S.: The Global Streamflow Indices and Metadata Archive (GSIM)- Part 1: The production of a daily streamflow archive and metadata, Earth Syst. Sci. Data, 10(2), 765–785, doi:10.5194/essd-10-765-2018, 2018.

Donohue, R. J., Roderick, M. L. and McVicar, T. R.: On the importance of including vegetation dynamics in Budyko's hydrological model, Hydrol. Earth Syst. Sci., 11(2), 983–995, doi:10.5194/hess-11-983-2007, 2007.

745   Duan, Q., Schaake, J., Andréassian, V., Franks, S., Goteti, G., Gupta, H. V., Gusev, Y. M., Habets, F., Hall, a., Hay, L., Hogue, T., Huang, M., Leavesley, G., Liang, X., Nasonova, O. N., Noilhan, J., Oudin, L., Sorooshian, S., Wagener, T. and Wood, E. F.: Model Parameter Estimation Experiment (MOPEX): An overview of science strategy and major results from

the second and third workshops, J. Hydrol., 320(1–2), 3–17, doi:10.1016/j.jhydrol.2005.07.031, 2006.

Eichinger, W. E., Parlange, M. B. and Stricker, H.: On the concept of equilibrium evaporation and the value of the Priestley-

750 Taylor coefficient, Water Resour. Res., 32(1), 161–164, doi:10.1029/95WR02920, 1996.

EMBRAPA: Sistema brasileiro de classificação de solos., 2018.

Fan, Y., Li, H. and Miguez-Macho, G.: Global patterns of groundwater table depth, Science (80-.)., 339(6122), 940–943, doi:10.1126/science.1229881, 2013.

FAO: World reference base for soil resources 2014. International soil classification system for naming soils and creating

755 legends for soil maps., 2014.

Forzieri, G., Alkama, R., Miralles, D. G. and Cescatti, A.: Response to Comment on "Satellites reveal contrasting responses of regional climate to the widespread greening of Earth," Science (80-.)., 360(6394), 1180–1184, doi:10.1126/science.aap9664, 2018.

Gadelha, A. N., Coelho, V. H. R., Xavier, A. C., Barbosa, L. R., Melo, D. C. D., Xuan, Y., Huffman, G. J., Petersen, W. A.

760 and Almeida, C. das N.: Grid box-level evaluation of IMERG over Brazil at various space and time scales, Atmos. Res., 218(October 2018), 231–244, doi:10.1016/j.atmosres.2018.12.001, 2019.

Gibbs, H. K., Ruesch, A. S., Achard, F., Clayton, M. K., Holmgren, P., Ramankutty, N. and Foley, J. A.: Tropical forests were the primary sources of new agricultural land in the 1980s and 1990s, Proc. Natl. Acad. Sci., 107(38), 16732–16737, doi:10.1073/PNAS.0910275107, 2010.

765 Gibbs, H. K., Rausch, L., Munger, J., Schelly, I., Morton, D. C., Noojipady, P., Barreto, P., Micol, L., Walker, N. F., Gibbs, B. H. K., Rausch, L., Munger, J., Schelly, I., Morton, D. C., Noojipady, P., Barreto, P., Micol, L., Walker, N. F., Amazon, B. and Cerrado, E.: Brazil's Soy Moratorium, Sci. - Policy Forum Environ. Dev., 347(6220), 377–378, doi:10.1126/science.aaa0181, 2014.

Gleeson, T., Moosdorf, N., Hartmann, J. and van Beek, L. P. H.: A glimpse beneath earth's surface: GLobal HYdrogeology

770 MaPS (GLHYMPS) of permeability and porosity, Geophys. Res. Lett., 41(11), 3891–3898, doi:10.1002/2014GL061184.Received, 2014.

Grant, S. A.: Hydraulic Properties, Temperature Effects, Encycl. Soils Environ., 4, 207–211, doi:10.1016/B0-12-348530-4/00379-9, 2005.

Groenendyk, D. G., Ferré, T. P. A., Thorp, K. R. and Rice, A. K.: Hydrologic-process-based soil texture classifications for

775 improved visualization of landscape function, PLoS One, 10(6), 1–17, doi:10.1371/journal.pone.0131299, 2015.

Guo, X., Zhang, H., Kang, L., Du, J., Li, W. and Zhu, Y.: Quality control and flux gap filling strategy for Bowen ratio method: Revisiting the Priestley-Taylor evaporation model, Environ. Fluid Mech., 7(5), 421–437, doi:10.1007/s10652-007-9033-8, 2007.

Gupta, H. V., Perrin, C., Blöschl, G., Montanari, a., Kumar, R., Clark, M. and Andréassian, V.: Large-sample hydrology: A

780 need to balance depth with breadth, Hydrol. Earth Syst. Sci., 18(2), 463–477, doi:10.5194/hess-18-463-2014, 2014.

Hargreaves, G. H.: Moisture Availability and Crop Production, Trans. ASAE, 18(5), 0980–0984, doi:10.13031/2013.36722,

1975.

Hargreaves, G. H. and Allen, R. G.: History and evaluation of Hargreaves evapotranspiration equation, J. Irrig. Drain. Eng., 129(1), 53–63, doi:10.1061/(ASCE)0733-9437(2004)130:5(447.2), 2003.

785   Hartmann, J. and Moosdorf, N.: The new global lithological map database GLiM: A representation of rock properties at the Earth surface, Geochemistry, Geophys. Geosystems, 13(12), 1–37, doi:10.1029/2012GC004370, 2012.

Hersbach, H., Bell, B., Berrisford, P., Hirahara, S., Horányi, A., Muñoz-Sabater, J., Nicolas, J., Peubey, C., Radu, R., Schepers, D., Simmons, A., Soci, C., Abdalla, S., Abellan, X., Balsamo, G., Bechtold, P., Biavati, G., Bidlot, J., Bonavita, M., De Chiara, G., Dahlgren, P., Dee, D., Diamantakis, M., Dragani, R., Flemming, J., Forbes, R., Fuentes, M., Geer, A.,

790   Haimberger, L., Healy, S., Hogan, R. J., Hólm, E., Janisková, M., Keeley, S., Laloyaux, P., Lopez, P., Lupu, C., Radnoti, G., de Rosnay, P., Rozum, I., Vamborg, F., Villaume, S. and Thépaut, J. N.: The ERA5 global reanalysis, Q. J. R. Meteorol. Soc., 146(730), 1999–2049, doi:10.1002/qj.3803, 2020.

Hou, A. Y., Kakar, R. K., Neeck, S., Azarbarzin, A. A., Kummerow, C. D., Kojima, M., Oki, R., Nakamura, K. and Iguchi, T.: The global precipitation measurement mission, Bull. Am. Meteorol. Soc., 95(5), 701–722, doi:10.1175/BAMS-D-13-

795   00164.1, 2014.

Huffman, G. J., Adler, R. F., Bolvin, D. T., Gu, G., Nelkin, E. J., Bowman, K. P., Hong, Y., Stocker, E. F. and Wolff, D. B.: The TRMM Multisatellite Precipitation Analysis (TMPA): Quasi-global, multiyear, combined-sensor precipitation estimates at fine scales, J. Hydrometeorol., 8(1), 38–55, doi:10.1175/JHM560.1, 2007.

Huntingford, C., Marsh, T., Scaife, A. A., Kendon, E. J., Hannaford, J., Kay, A. L., Lockwood, M., Prudhomme, C.,

800   Reynard, N. S., Parry, S., Lowe, J. A., Screen, J. A., Ward, H. C., Roberts, M., Stott, P. A., Bell, V. A., Bailey, M., Jenkins, A., Legg, T., Otto, F. E. L., Massey, N., Schaller, N., Slingo, J. and Allen, M. R.: Potential influences on the United Kingdom's floods of winter 2013/14, Nat. Clim. Chang., 4(9), 769–777, doi:10.1038/nclimate2314, 2014.

Kousky, V. E., Kagano, M. T. and Cavalcanti, I. F. a: A review of the Southern Oscillation: oceanic-atmospheric circulation changes and related rainfall anomalies, Tellus A, 36 A(5), 490–504, doi:10.1111/j.1600-0870.1984.tb00264.x, 1984.

805   Lima, C. H. R. and AghaKouchak, A.: Droughts in Amazonia: Spatiotemporal Variability, Teleconnections, and Seasonal Predictions, Water Resour. Res., 53(12), 10824–10840, doi:10.1002/2016WR020086, 2017.

Lo, M. H., Famiglietti, J. S., Yeh, P. J. F. and Syed, T. H.: Improving parameter estimation and water table depth simulation in a land surface model using GRACE water storage and estimated base flow data, Water Resour. Res., 46(5), 1–15, doi:10.1029/2009WR007855, 2010.

810   Lyon, S. W. and Troch, P. A.: Development and application of a catchment similarity index for subsurface flow, Water Resour. Res., 46(3), 1–13, doi:10.1029/2009WR008500, 2010.

Maes, W. H., Gentine, P., Verhoest, N. E. C. and Miralles, D. G.: Potential evaporation at eddy-covariance sites across the globe, Hydrol. Earth Syst. Sci. Discuss., (i), 1–38, doi:10.5194/hess-2018-470, 2018.

Maidment, D. R.: Arc Hydro: GIS for Water Resources., 2002.

815   Martens, B., Miralles, D. G., Lievens, H., Van Der Schalie, R., De Jeu, R. A. M., Fernández-Prieto, D., Beck, H. E., Dorigo,

W. A. and Verhoest, N. E. C.: GLEAM v3: Satellite-based land evaporation and root-zone soil moisture, Geosci. Model Dev., 10(5), 1903–1925, doi:10.5194/gmd-10-1903-2017, 2017.

McMahon, T. A., Peel, M. C., Lowe, L., Srikanthan, R. and McVicar, T. R.: Estimating actual, potential, reference crop and pan evaporation using standard meteorological data: A pragmatic synthesis, Hydrol. Earth Syst. Sci., 17(4), 1331–1363,
820 doi:10.5194/hess-17-1331-2013, 2013.

Melo, D. D. C. D., Xavier, A. C., Bianchi, T., Oliveira, P. T. S., Scanlon, B. R., Lucas, M. C. and Wendland, E.: Performance evaluation of rainfall estimates by TRMM Multi-satellite Precipitation Analysis 3B42V6 and V7 over Brazil, J. Geophys. Res. Atmos., 120(18), 9426–9436, doi:10.1002/2015JD023797, 2015.

Monteiro, L. A., Sentelhas, P. C. and Pedra, G. U.: Assessment of NASA/POWER satellite-based weather system for
825 Brazilian conditions and its impact on sugarcane yield simulation, Int. J. Climatol., 38(3), 1571–1581, doi:10.1002/joc.5282, 2018.

Mukherjee, S., Joshi, P. K., Mukherjee, S., Ghosh, A., Garg, R. D. and Mukhopadhyay, A.: Evaluation of vertical accuracy of open source Digital Elevation Model (DEM), Int. J. Appl. Earth Obs. Geoinf., 21(1), 205–217, doi:10.1016/j.jag.2012.09.004, 2012.

830 Nobre, A. D., Cuartas, L. A., Hodnett, M., Rennó, C. D., Rodrigues, G., Silveira, A., Waterloo, M. and Saleska, S.: Height Above the Nearest Drainage - a hydrologically relevant new terrain model, J. Hydrol., 404(1–2), 13–29, doi:10.1016/j.jhydrol.2011.03.051, 2011.

Oliveira, P. T. S., Almagro, A., Pitaluga, F., Meira Neto, A. A., Durcik, M. and Troch, P. A.: CABra: a novel large-scale dataset for Brazilian catchments, in AGU Fall Meeting, p. 12138., 2020.

835 Pires, G. F., Abrahão, G. M., Brumatti, L. M., Oliveira, L. J. C., Costa, M. H., Liddicoat, S., Kato, E. and Ladle, R. J.: Increased climate risk in Brazilian double cropping agriculture systems: Implications for land use in Northern Brazil, Agric. For. Meteorol., 228–229, 286–298, doi:10.1016/j.agrformet.2016.07.005, 2016.

Priestley, C. H. B. and Taylor, R. J.: On the Assessment of Surface Heat Flux and Evaporation Using Large-Scale Parameters, Mon. Weather Rev., 100(2), 81–92, doi:10.1175/1520-0493(1972)100<0081:otaosh>2.3.co;2, 1972.

840 Ren, H., Hou, Z., Huang, M., Bao, J., Sun, Y., Tesfa, T. and Ruby Leung, L.: Classification of hydrological parameter sensitivity and evaluation of parameter transferability across 431 US MOPEX basins, J. Hydrol., 536, 92–108, doi:10.1016/j.jhydrol.2016.02.042, 2016.

Roderick, M. L., Sun, F., Lim, W. H. and Farquhar, G. D.: A general framework for understanding the response of the water cycle to global warming over land and ocean, Hydrol. Earth Syst. Sci., 18(5), 1575–1589, doi:10.5194/hess-18-1575-2014,
845 2014.

Rodrigues, D. B. B., Gupta, H. V., Serrat-Capdevila, A., Oliveira, P. T. S., Mario Mendiondo, E., Maddock, T. and Mahmoud, M.: Contrasting American and Brazilian systems for water allocation and transfers, J. Water Resour. Plan. Manag., 141(7), 1–11, doi:10.1061/(ASCE)WR.1943-5452.0000483, 2015.

Santos, H. G., Carvalho Júnior, W., Dart, R. O., Áglio, M. L. D., Sousa, J. S., Pares, J. G., Fontana, A., Martins, A. L. S. and

850   Oliveira, A. P. O.: O novo mapa de solos do Brasil: legenda atualizada, Embrapa Solos, 67 [online] Available from: https://www.embrapa.br/busca-de-publicacoes/-/publicacao/920267/o-novo-mapa-de-solos-do-brasil-legenda-atualizada, 2011.

Sawicz, K., Wagener, T., Sivapalan, M., Troch, P. A. and Carrillo, G.: Catchment classification: empirical analysis of hydrologic similarity based on catchment function in the eastern USA, Hydrol. Earth Syst. Sci., 15, 2895–2911,

855   doi:10.5194/hess-15-2895-2011, 2011.

Saxton, K. E. and Rawls, W. J.: Soil Water Characteristic Estimates by Texture and Organic Matter for Hydrologic Solutions, Soil Sci. Soc. Am. J., 70(5), 1569–1578, doi:10.2136/sssaj2005.0117, 2006.

Saxton, K. E., Rawls, W. J., Romberger, J. S. and Papendick, R. I.: Estimating Generalized Soil-water Characteristics from Texture, Soil Sci. Soc. Am. J., 50(4), 1031–1036, doi:10.2136/sssaj1986.03615995005000040039x, 1986.

860   Schaake, J., Cong, S. and Duan, Q.: The US mopex data set, IAHS-AISH Publ., (307), 9–28, 2006.

Schulzweida, U.: CDO User guide (1.9.6), , 2015, doi:10.5281/zenodo.2558193, 2019.

Schumacher, D. L., Keune, J., van Heerwaarden, C. C., Vilà-Guerau de Arellano, J., Teuling, A. J. and Miralles, D. G.: Amplification of mega-heatwaves through heat torrents fuelled by upwind drought, Nat. Geosci., 12(9), 712–717, doi:10.1038/s41561-019-0431-6, 2019.

865   Shirazi, M. A. and Boersma, L.: A Unifying Quantitative Analysis of Soil Texture, Soil Sci. Soc. Am. J., 48(1), 142–147, doi:10.2136/sssaj1984.03615995004800010026x, 1984.

Shuttleworth, W. J.: Evaporation, in Handbook of Hydrology, edited by D. R. Maidment, p. 824, McGraw-Hill Education., 1996.

Souza, R., Feng, X., Antonino, A., Montenegro, S., Souza, E. and Porporato, A.: Vegetation response to rainfall seasonality

870   and interannual variability in tropical dry forests, Hydrol. Process., 30(20), 3583–3595, doi:10.1002/hyp.10953, 2016.

Spera, S. A., Galford, G. L., Coe, M. T., Macedo, M. N. and Mustard, J. F.: Land-use change affects water recycling in Brazil's last agricultural frontier, Glob. Chang. Biol., 22(10), 3405–3413, doi:10.1111/gcb.13298, 2016.

Strahler, A. N.: Hypsometric Area-Altitude Analysis of Erosional Topography, Bull. Geol. Soc. Am., 63(11), 1117–1142, doi:10.1130/0016-7606(1952)63, 1952.

875   Strahler, A. N.: Quantitative Analysis of Watershed Geomorphology, Trans. ASAE, 38(6), 913–920, 1957.

Tetzlaff, D., Carey, S. K., McNamara, J. P., Laudon, H. and Soulsby, C.: The essential value of long-term experimental data for hydrology and water management, Water Resour. Res., 53(4), 2598–2604, doi:10.1002/2017WR020838, 2017.

Tucker, C. J.: Red and Photographic Infrared l , lnear Combinations for Monitoring Vegetation, Remote Sens. Environ., 8, 127–150, 1979.

880   Twarakavi, N. K. C., Šimůnek, J. and Schaap, M. G.: Can texture-based classification optimally classify soils with respect to soil hydraulics?, Water Resour. Res., 46(1), doi:10.1029/2009WR007939, 2010.

UNEP and ANA: GEO Brazil Water Resources., 2007.

Vaze, J., Teng, J. and Spencer, G.: Impact of DEM accuracy and resolution on topographic indices, Environ. Model. Softw.,

25(10), 1086–1098, doi:10.1016/j.envsoft.2010.03.014, 2010.

885 Wagener, T., Sivapalan, M., Troch, P. and Woods, R.: Catchment Classification and Hydrologic Similarity, Geogr. Compass, 1(4), 901–931, 2007.

Wechsler, S. P.: Uncertainties associated with digital elevation models for hydrologic applications : a review, Hydrol. Earth Syst. Sci., 11(4), 1481–1500, 2007.

Westerberg, I. K. and McMillan, H. K.: Uncertainty in hydrological signatures, Hydrol. Earth Syst. Sci., 19, 3951–3968,
890 doi:10.5194/hess-19-3951-2015, 2015.

Whited, D. C., Lorang, M. S., Harner, M. J., Hauer, F. R., Kimball, J. S. and Stanford, J. A.: Climate, hydrologic disturbance, and succession: Drivers of floodplain pattern, Ecology, 88(4), 940–953, doi:10.1890/05-1149, 2007.

WMO: Guide to the Global Observing System., 2010.

Woods, R. A.: Analytical model of seasonal climate impacts on snow hydrology: Continuous snowpacks, Adv. Water
895 Resour., 32(10), 1465–1481, doi:10.1016/j.advwatres.2009.06.011, 2009.

Xavier, A. C., King, C. W. and Scanlon, B. R.: Daily gridded meteorological variables in Brazil (1980-2013), Int. J. Climatol., 2659(October 2015), 2644–2659, doi:10.1002/joc.4518, 2015.

Yadav, M., Wagener, T. and Gupta, H. V.: Regionalization of constraints on expected watershed response behavior for improved predictions in ungauged basins, Adv. Water Resour., 30, 1756–1774, doi:10.1016/j.advwatres.2007.01.005, 2007.

900 Yamazaki, D., Ikeshima, D., Tawatari, R., Yamaguchi, T., O'Loughlin, F., Neal, J. C., Sampson, C. C., Kanae, S. and Bates, P. D.: A high-accuracy map of global terrain elevations, Geophys. Res. Lett., 44(11), 5844–5853, doi:10.1002/2017GL072874, 2017.

Zhang, Y., Peña-Arancibia, J. L., McVicar, T. R., Chiew, F. H. S., Vaze, J., Liu, C., Lu, X., Zheng, H., Wang, Y., Liu, Y. Y., Miralles, D. G. and Pan, M.: Multi-decadal trends in global terrestrial evapotranspiration and its components, Sci. Rep.,
905 6(December 2015), 1–12, doi:10.1038/srep19124, 2016.

Zhou, Q. and Liu, X.: Analysis of errors of derived slope and aspect related to DEM data properties, Comput. Geosci., 30(4), 369–378, doi:10.1016/j.cageo.2003.07.005, 2004.